Remote effect of anisotropy in electrical conductivity or magnetic permeability on dynamo action

Franck Plunian[1]†, and Paul Gomez[2] and Thierry Alboussière[2]

[1]Université Grenoble Alpes, Université Savoie Mont Blanc, CNRS, IRD, IFSTTAR, ISTerre, 38000 Grenoble, France

[2]Université Lyon 1, ENS de Lyon, CNRS, Laboratoire de Géologie de Lyon, Lyon 69622, France

(Received xx; revised xx; accepted xx)

We demonstrate that a localized simple shear in an electrically conducting fluid can generate dynamo action, due to the presence of a distant solid wall with anisotropic electrical conductivity or magnetic permeability. Three cylindrical geometries are considered, depending on the position of the solid wall relative to the shear zone. The wall can be either (a) internal, (b) external, or (c) both internal and external, relative to the shear zone. For each of the three geometries, the dynamo threshold is derived analytically. Results are presented with experimental applications in mind, corresponding to present, past or future dynamo experiments. We also consider an application to the Earth's core, assuming anisotropic electrical conductivity in the inner core and some shear in the tangent cylinder.

Key words: Magnetohydrodynamics, Dynamo effect, Anisotropy, Axisymmetry, Dynamo experiment, Geodynamo

1. Introduction

1.1. *Remote effect in dynamo action*

In dynamo theory, the self-generation of a magnetic field from the motion of an electrically conducting fluid is generally thought to be localised in space, as suggested by the fast dynamo mechanism in which the stretching, twisting, and folding of the magnetic field by the fluid motion, all occur at the same place (Vainshtein & Zel'dovich 1972; Childress & Gilbert 1995). When the magnetic Reynolds number is high, the dynamo process then takes place within thin magnetic boundary layers, as is well documented for the Ponomarenko and Roberts dynamos (Gilbert 1988; Ruzmaikin *et al.* 1988; Soward 1987; Gilbert 2003; Tobias 2021). However, this aspect of spatial confinement is not mandatory, as is the case, for example, with the Herzenberg dynamo (Herzenberg 1958), which consists of two differential rotations (ω^2-dynamo) situated at a certain distance from one another. Another example is the mean-field dynamo (Steenbeck *et al.* 1966; Krause & Rädler 1980), which is typically composed of two α-effects (α^2-dynamo) or one α-effect and one differential rotation ($\alpha\omega$-dynamo). Each mechanism considered alone (a simple differential rotation ω, or an α-effect) cannot produce the dynamo on its own,

† Email address for correspondence: Franck.Plunian@univ-grenoble-alpes.fr

but the interplay of two of them, α^2, or $\alpha\omega$, is sufficient to generate a magnetic field, even if they are distant from each other. If they do not operate in the same location, the transmission of electric currents from one place to another requires them to be electrically connected – generally considered to be part of the same electrically conducting medium. Such interplay of two distant mechanisms is also believed to be at work in the solar dynamo. The tachocline at the basis of the convection zone is the obvious site for differential rotation, while the α-effect is considered to be located either near the surface, or distributed throughout the convection zone (Weiss & Thompson 2009; Jones *et al.* 2010). Of course, the greater the distance between the two locations, the less efficient the dynamo will be. To take a simple example, in the disc-dynamo of Bullard (1955), two mechanisms are also at work: the shear between the rotating rim of the disc and the wire, and the effect of the wound part of the wire (the loop) which is at some distance from the disc. The dynamo threshold expressed in terms of the angular velocity of the disc is $\Omega = R/M$ where R and M are respectively the electric resistance of the wire and the mutual inductance between the loop and the disc (Moffatt 1978). If we denote the distance between the disc and the loop by d, then M decreases and R increases linearly with d, implying that the dynamo threshold increases as d^2.

1.2. *Anisotropic dynamo*

After several decades during which the experimental implementation of the Bullard dynamo was considered impossible, mainly due to the high resistance of the electrical contact between the disc and the wire (Rädler & Rheinhardt 2002), a decisive breakthrough was achieved by Priede & Avalos-Zúñiga (2013), who, instead of a single wire, proposed using a spiral-segmented disc and an electrical contact extending around the entire circumference of the disc. In their theroretical model, the spiral-segmented disc is replaced by a material exhibiting anisotropic electrical conductivity. As Cowling's anti-dynamo theorem (Cowling 1934) no longer applies, it can then be assumed that the magnetic mode is axisymmetric — a common assumption in subsequent models of anisotropic dynamos (Alboussière *et al.* 2020; Plunian & Alboussière 2020). The concept of the anisotropic dynamo has been independently confirmed by two experimental demonstrations based on different geometries (Alboussière *et al.* 2022; Avalos-Zúñiga & Priede 2023).

In the anisotropic dynamo, two distinct mechanisms are at work; one being the deflection of electric currents by the presence of a material having an anisotropic electrical conductivity – we speak of an anisotropic material; the other being, in its simplest form, shear. Once again, simple shearing cannot generate a magnetic field; it is the combination of shear with the anisotropic material that creates the dynamo effect. We note that an anisotropy of magnetic permeability also works (Plunian & Alboussière 2021), implying a deflection of the magnetic field instead. Furthermore, there is a necessary condition between the direction of anisotropy and that of shear, just as in Bullard's disc-dynamo, the direction of rotation of the disc, and that of the wire winding. In other words, for a given anisotropy, there is only one direction of shear for which the dynamo works.

In the Fury dynamo experiment (Alboussière *et al.* 2022), a rotor rotates inside a stator, both of which are cylindrical in shape, and made of the same anisotropic material. Although a layer of an electrically conducting fluid is sandwiched between the rotor and the stator to ensure good electric contact, it is so thin (1% of the rotor radius) that it can be disregarded when calculating the dynamo threshold. The angular velocity profile thus corresponds to a Heaviside step function. A smooth profile also works and has been studied in the context of fast dynamo action (Plunian & Alboussière 2022), and spiral galaxies (Gomez *et al.* 2025). As part of the preparation for another dynamo experiment, the effect of the fluid layer thickness was also investigated (Plunian *et al.*

2025). Within a fluid, because the electrical conductivity is isotropic, the electric currents are not deflected, and therefore do not contribute directly to the dynamo mechanism. The dynamo threshold thus inevitably increases with the fluid thickness, but still works even in the limit of infinite thickness (Plunian & Alboussière 2023).

In these studies, the shear was always taken in contact with the anisotropic material, even in the cases involving a fluid. This raises the question of whether the dynamo would work if, instead, the shear occurred within the fluid, and therefore at some distance from the anisotropic material. In this case, the electric currents would be deflected only at a certain distance from the shear, making the dynamo more difficult to achieve. This is, however, of fundamental importance, as shear does not necessarily occur at the walls of a fluid.

1.3. *Outline*

We will examine three configurations based on the number of solid components: (a) one rotor, (b) one stator, (c) one rotor and one stator, all made from the same anisotropic material. Space is therefore divided into three domains in cases (a) and (b), and four domains in case (c), as shown in figure 1. The increase of the number of domains increases the number of boundary conditions (section 3), which leads to a system of eight (resp. twelve) equations to be solved in cases (a) and (b) (resp. (c)), as derived in section 4. An explicit expression for the dynamo threshold is obtained in each of these three cases (section 5), and a number of checks can be carried out, on the basis of previous studies or by comparing case (c) with case (a) or (b), as outlined in section 6. Finally, in section 7, we investigate how the dynamo threshold varies with the distance between the shear and the anisotropic material for three applications chosen for their relevance to past or future experiments. We also estimate the degree of anisotropy that would be necessary to produce a dynamo effect from simple shear within the Earth's liquid outer core iron, if the inner core were made of anisotropic solid iron.

2. General formulation

2.1. *Shear*

To solve the problem analytically, the shear within the fluid layer will be treated in its simplest form, namely a Heaviside step function, with one part being at rest and the other one having a non-zero angular velocity (figure 1). To implement the remote effect of electrical conductivity (or magnetic permeability) anisotropy, we will consider one rotor (case (a)), one stator (case (b)), or both one rotor and one stator (case (c)), located at a certain distance e (case (a) and (b)), or e_1 and $e - e_1$ (case (c)), from the shear (figure 1).

In cases (a) and (b), space is therefore divided into three cylindrical regions: $r < R, R < r < R + e$ and $r > R + e$, where r is the radial coordinate, as illustrated in figures 1a and 1b. Only one part, the rotor in case (a), the stator in case (b), is made of an anisotropic material. In case (a), the fluid inner part ($R < r < R + e$) rotates at the same angular velocity Ω as the rotor, while the fluid outer part ($r > R + e$) is at rest. In case (b), the fluid outer part ($R < r < R + e$) is at rest as the stator, while the inner part ($r < R$) rotates at angular velocity Ω. Therefore, in both cases, the shear occurs in the fluid layer at a distance e from the anisotropic medium, namely at (a) $r = R + e$, or (b) $r = R$.

In case (c), space is divided into four cylindrical regions: $r < R, R < r < R+e_1, R+e_1 < r < R + e$ and $r > R + e$, the fluid layer corresponding to the two intermediate parts $R < r < R+e_1$ and $R+e_1 < r < R+e$, as illustrated in figure 1c. Both the rotor ($r < R$)

and the stator ($r > R + e$) are made of the same anisotropic material. The inner part of the fluid layer ($R < r < R + e_1$) rotates at the same angular velocity as the rotor, while the outer part ($R + e_1 < r < R + e$) is at rest as the stator. The shear then occurs at a distance e_1 from the rotor and $e - e_1$ from the stator, namely at $r = R + e_1$.

In cases (a) and (b), setting $e = 0$ corresponds to a shear at the interface $r = R$, between the fluid layer and the anisotropic material, which has already been studied in Plunian & Alboussière (2023). In case (c), setting $e_1 = 0$, or $e - e_1 = 0$, corresponds to the two cases studied in Plunian *et al.* (2025), with a shear at the interface between the fluid layer and either, the rotor at $r = R$, or the stator at $r = R + e_1$. In cases (a) and (b), for $e \gg 1$ the shear is pushed to an infinitely large distance from the anisotropic material, which makes the dynamo effect impossible. We therefore expect that an increase in e will lead to an increase in the dynamo threshold. In case (c), similarly, we expect an increase of the dynamo threshold for $e \gg e_1 \gg 1$. For the applications discussed in section 7, e will be of the same order of magnitude as the rotor radius $e = O(R)$.

The velocity field is given by $\boldsymbol{U} = r\tilde{\Omega}\boldsymbol{e}_\theta$, with

$$\tilde{\Omega}^{(a)} = \begin{cases} \Omega \\ \Omega \\ 0 \end{cases}, \quad \tilde{\Omega}^{(b)} = \begin{cases} \Omega \\ 0 \\ 0 \end{cases}, \quad \text{for} \begin{cases} 0 < r < R \\ R < r < R + e \\ r > R + e \end{cases}, \tag{2.1a}$$

$$\tilde{\Omega}^{(c)} = \begin{cases} \Omega \\ \Omega \\ 0 \\ 0 \end{cases}, \quad \text{for} \begin{cases} 0 < r < R \\ R < r < R + e_1 \\ R + e_1 < r < R + e \\ r > R + e \end{cases}, \tag{2.1b}$$

where $(\boldsymbol{e}_r, \boldsymbol{e}_\theta, \boldsymbol{e}_z)$ and (r, θ, z) are unit basis vectors and coordinates in cylindrical geometry, and where the superscripts $(a), (b)$ and (c) correspond to the three cases introduced above and depicted in figure 1.

2.2. *Anisotropy*

In each domain, we define two electrical conductivities and two magnetic permeabilities, $\sigma^{\parallel}$ and $\mu^{\parallel}$ in a given direction $\boldsymbol{q}$, $\sigma^{\perp}$ and $\mu^{\perp}$ in the directions perpendicular to $\boldsymbol{q}$, where $\boldsymbol{q}$ is a unit vector. In the direction parallel to $\boldsymbol{q}$, Ohm's law and the relation between $\boldsymbol{H}$ and $\boldsymbol{B}$ are written in the form† $\boldsymbol{J} \cdot \boldsymbol{q} = \sigma^{\parallel}(\boldsymbol{E} \cdot \boldsymbol{q})$ and $\boldsymbol{B} \cdot \boldsymbol{q} = \mu^{\parallel}(\boldsymbol{H} \cdot \boldsymbol{q})$, while in the directions perpendicular to $\boldsymbol{q}$, they are written as $\boldsymbol{J} - (\boldsymbol{J} \cdot \boldsymbol{q})\boldsymbol{q} = \sigma^{\perp}(\boldsymbol{E} - (\boldsymbol{E} \cdot \boldsymbol{q})\boldsymbol{q})$ and $\boldsymbol{B} - (\boldsymbol{B} \cdot \boldsymbol{q})\boldsymbol{q} = \mu^{\perp}(\boldsymbol{H} - (\boldsymbol{H} \cdot \boldsymbol{q})\boldsymbol{q})$. This leads to two symmetric tensors, $[\sigma_{ij}]$ for the electrical conductivity and $[\mu_{ij}]$ for the magnetic permeability, defined by

$$[\sigma_{ij}] = \sigma^{\perp}\delta_{ij} + (\sigma^{\parallel} - \sigma^{\perp})q_i q_j, \qquad [\mu_{ij}] = \mu^{\perp}\delta_{ij} + (\mu^{\parallel} - \mu^{\perp})q_i q_j. \tag{2.2a, b}$$

For a fluid, with isotropic electrical conductivity σ_F and magnetic permeability μ_F, the expressions $(2.2a, b)$ remain valid, with $\sigma^{\perp} = \sigma^{\parallel} = \sigma_F$ and $\mu^{\perp} = \mu^{\parallel} = \mu_F$. Anticipating a renormalization of the electrical conductivity and magnetic permeability by $\sigma^{\perp}$ and $\mu^{\perp}$, it is then useful to rewrite $(2.2a, b)$ as follows,

$$[\sigma_{ij}] = \sigma^{\perp}\, \tilde{\varphi}_\sigma \left(\delta_{ij} - \frac{\tilde{\sigma}}{1 + \tilde{\sigma}} q_i q_j\right), \qquad [\mu_{ij}] = \mu^{\perp}\, \tilde{\varphi}_\mu \left(\delta_{ij} - \frac{\tilde{\mu}}{1 + \tilde{\mu}} q_i q_j\right), \tag{2.3a, b}$$

† where $\boldsymbol{J}$, $\boldsymbol{E}$, $\boldsymbol{H}$ and $\boldsymbol{B}$ denote the current density, the electric field, the magnetic field and the magnetic induction, respectively.

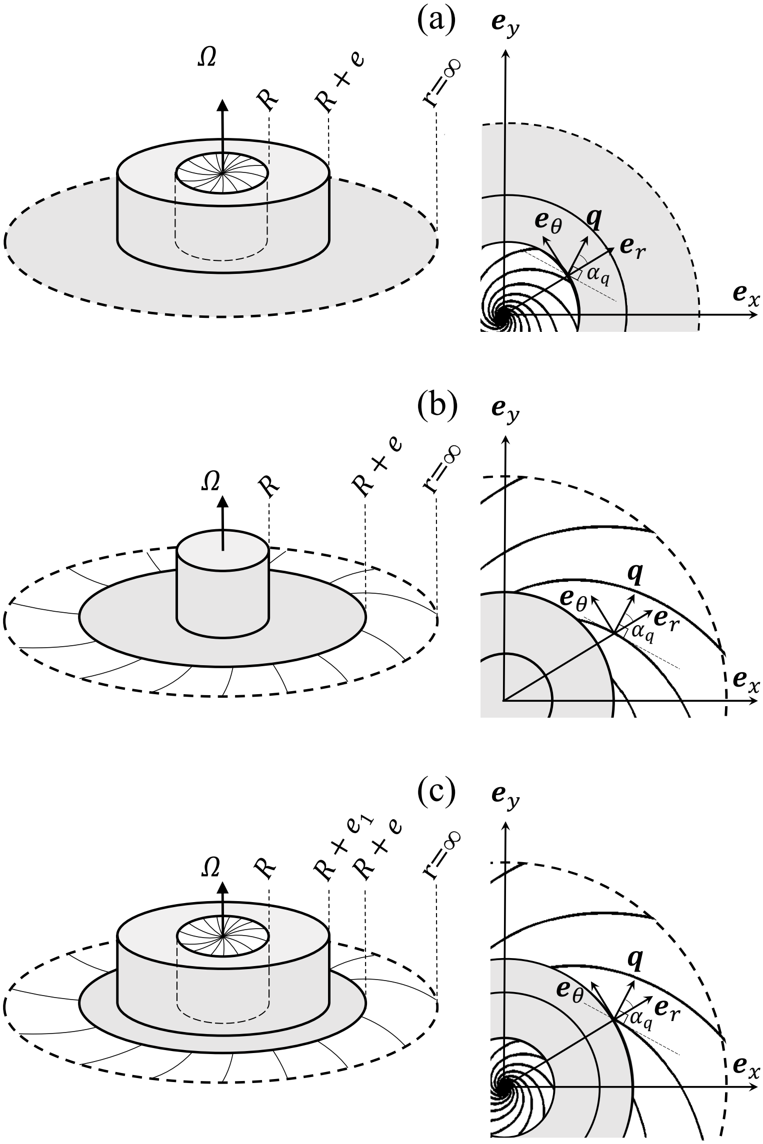

FIGURE 1. A non-zero angular velocity Ω is represented by a vertical elevation. The fluid layer is represented in grey and divided into two parts: one is rotating, the other is at rest. The anisotropic material is represented with logarithmic spirals, the rotor in case (a), the stator in case (b), both rotor and stator in case (c).
- Case (a): The fluid inner part ($R < r < R + e$) rotates at the same angular velocity as the rotor ($r < R$). The fluid outer part ($r > R + e$) is at rest. Shear occurs at radius $r = R + e$.
- Case (b): The fluid ($r < R + e$) is surrounded by a stator ($r > R + e$) at rest. The fluid inner part ($r < R$) rotates, while the fluid outer part ($R < r < R + e$) is at rest. Shear occurs at radius $r = R$.
- Case (c): The fluid layer is sandwiched between a rotor ($r < R$) and a stator ($r > R + e$). The fluid inner part ($R < r < R + e_1$) rotates at the same angular velocity as the rotor. The fluid outer part ($R + e_1 < r < R + e$) is at rest as the stator. Shear occurs at radius $r = R + e_1$.
The logarithmic spirals in the rotor (case (a) and (c)) and the stator (case (b) and (c)) correspond to the direction of the electric current (resp. magnetic field) for $\sigma^\perp \gg \sigma^\parallel$ (resp. $\mu^\perp \gg \mu^\parallel$), which are perpendicular to $\boldsymbol{q}$.

with, in case (a),

$$\tilde{\varphi}_\sigma^{(a)} = \begin{cases} 1 \\ \varphi_\sigma \\ \varphi_\sigma \end{cases}, \; \tilde{\sigma}^{(a)} = \begin{cases} \sigma \\ 0 \\ 0 \end{cases}, \; \tilde{\varphi}_\mu^{(a)} = \begin{cases} 1 \\ \varphi_\mu \\ \varphi_\mu \end{cases}, \; \tilde{\mu}^{(a)} = \begin{cases} \mu \\ 0 \\ 0 \end{cases}, \; \text{for} \begin{cases} r < R \\ R < r < R+e \\ r > R+e \end{cases}, \quad (2.4a-d)$$

in case (b),

$$\tilde{\varphi}_\sigma^{(b)} = \begin{cases} \varphi_\sigma \\ \varphi_\sigma \\ 1 \end{cases}, \; \tilde{\sigma}^{(b)} = \begin{cases} 0 \\ 0 \\ \sigma \end{cases}, \; \tilde{\varphi}_\mu^{(b)} = \begin{cases} \varphi_\mu \\ \varphi_\mu \\ 1 \end{cases}, \; \tilde{\mu}^{(b)} = \begin{cases} 0 \\ 0 \\ \mu \end{cases}, \; \text{for} \begin{cases} r < R \\ R < r < R+e \\ r > R+e \end{cases}, \quad (2.5a-d)$$

in case (c)

$$\tilde{\varphi}_\sigma^{(c)} = \begin{cases} 1 \\ \varphi_\sigma \\ \varphi_\sigma \\ 1 \end{cases}, \quad \tilde{\sigma}^{(c)} = \begin{cases} \sigma \\ 0 \\ 0 \\ \sigma \end{cases}, \quad \tilde{\varphi}_\mu^{(c)} = \begin{cases} 1 \\ \varphi_\mu \\ \varphi_\mu \\ 1 \end{cases}, \quad \tilde{\mu}^{(c)} = \begin{cases} \mu \\ 0 \\ 0 \\ \mu \end{cases}, \quad \text{for} \begin{cases} r < R \\ R < r < R+e_1 \\ R+e_1 < r < R+e \\ r > R+e \end{cases}, \quad (2.6a-d)$$

and

$$\varphi_\sigma = \frac{\sigma_F}{\sigma^\perp}, \quad \sigma = \frac{\sigma^\perp}{\sigma^\parallel} - 1, \quad \varphi_\mu = \frac{\mu_F}{\mu^\perp}, \quad \mu = \frac{\mu^\perp}{\mu^\parallel} - 1. \quad (2.7a-d)$$

As in previous studies on the anisotropic dynamo (Plunian & Alboussière 2020, 2021, 2022, 2023; Plunian *et al.* 2025; Gomez *et al.* 2025), we choose $\boldsymbol{q}$ as a unit vector in the horizontal plane defined by

$$\boldsymbol{q} = c\ \boldsymbol{e}_r + s\ \boldsymbol{e}_\theta, \quad (2.8)$$

where $c = \cos\alpha_q$, $s = \sin\alpha_q$, with α_q a prescribed pitch angle. The vector $\boldsymbol{q}$ follows the direction of logarithmic spirals which are perpendicular to the ones depicted in figure 1 (see Ruderman & Ruzmaikin (1984); Alboussière *et al.* (2020) for an alternative expression in Cartesian geometry).

2.3. *Induction equation*

In the magnetohydrodynamic approximation, Maxwell's equations and Ohm's law take the following forms

$$\boldsymbol{H} = [\mu_{ij}]^{-1}\boldsymbol{B}, \quad (2.9a)$$
$$\nabla\cdot\boldsymbol{B} = 0, \quad (2.9b)$$
$$\boldsymbol{J} = \nabla\times\boldsymbol{H}, \quad (2.9c)$$
$$\partial_t\boldsymbol{B} = -\nabla\times\boldsymbol{E} \quad (2.9d)$$
$$\boldsymbol{J} = [\sigma_{ij}](\boldsymbol{E} + \boldsymbol{U}\times\boldsymbol{B}), \quad (2.9e)$$

leading to the induction equation,

$$\partial_t\boldsymbol{B} = \nabla\times(\boldsymbol{U}\times\boldsymbol{B}) - \nabla\times\left([\sigma_{ij}]^{-1}\nabla\times\left([\mu_{ij}]^{-1}\boldsymbol{B}\right)\right), \quad (2.10)$$

where

$$[\sigma_{ij}]^{-1} = \left(\tilde{\varphi}_\sigma\sigma^\perp\right)^{-1}(\delta_{ij} + \tilde{\sigma}q_iq_j), \qquad [\mu_{ij}]^{-1} = \left(\tilde{\varphi}_\mu\mu^\perp\right)^{-1}(\delta_{ij} + \tilde{\mu}q_iq_j). \quad (2.11a,b)$$

Equations (2.11a, b) have been derived from (2.3a, b) knowing that, for any unit vector $\boldsymbol{q}$ and any scalar quantity $X \neq -1$, we have

$$\left[\delta_{ij} - \frac{X}{1+X} q_i q_j\right]^{-1} = \delta_{ij} + X q_i q_j. \tag{2.12}$$

With regard to the induction equation (2.10), and for an isotropic material such that $[\sigma_{ij}]$ and $[\mu_{ij}]$ are reduced to scalar quantities, it has been shown, using duality arguments, that swapping the electrical conductivity and magnetic permeability leads to the same dynamo threshold, provided that there is a change of sign in the velocity field and that the boundary conditions of the conducting domain can also be swapped (infinitely conducting with ferromagnetic) (Favier & Proctor 2013; Marcotte *et al.* 2021). This demonstration can easily be generalised to the current case of an anisotropic material, and for the boundary conditions (3.1c-d) given in section 3.1. Consequently, we expect to have the same dynamo threshold by swapping σ and μ, φ_σ and φ_μ, Ω and $-\Omega$.

Since the velocity is stationary and independent of z and θ, we look for a magnetic induction in the form

$$\boldsymbol{B}(r)\exp(\gamma t + \mathrm{i}kz + im\theta), \tag{2.13}$$

where $\boldsymbol{B}(r)$ is the magnetic mode at vertical wave number k and azimuthal wave number m. In (2.13) a positive value of the real part of the magnetic growth rate γ is the signature of dynamo action, the dynamo threshold corresponding to $\Re\{\gamma\} = 0$. The present work is restricted to the axisymmetric mode $m = 0$, motivated by the fact that it does not involve azimuthal gradients and is therefore the least dissipative candidate. This is also consistent with previous experimental studies of anisotropic dynamo (Alboussière *et al.* 2022; Avalos-Zúñiga & Priede 2023) in which the magnetic field is indeed axisymmetric. As mentioned in section 1.2, the generation of an axisymmetric mode $m = 0$ is possible because in the anisotropic material the electric currents are deflected, implying that Cowling's antidynamo theorem (Cowling 1934) does not hold (Plunian & Alboussière 2020).

Replacing (2.1a), (2.1b) and (2.13) in (2.10), and after some algebra (see e.g. Plunian & Alboussière (2023)), one obtains the following equations for $B_r(r)$ and $B_\theta(r)$,

$$\tilde{\gamma} B_r = -(\sigma^\perp \mu^\perp)^{-1}\left[\tilde{\mu} c^2 k^2 B_r + (1+\tilde{\sigma} s^2) D_k(B_r) - cs(\tilde{\sigma} - \tilde{\mu}) k^2 B_\theta\right], \tag{2.14a}$$

$$\tilde{\gamma} B_\theta = -(\sigma^\perp \mu^\perp)^{-1}\left[\tilde{\sigma} c^2 k^2 B_\theta + (1+\tilde{\mu} s^2) D_k(B_\theta) - cs(\tilde{\sigma} - \tilde{\mu}) D_k(B_r)\right], \tag{2.14b}$$

where $\tilde{\gamma} = \tilde{\varphi}_\sigma \tilde{\varphi}_\mu \gamma$ is given by

$$\tilde{\gamma}^{(a)} = \gamma \begin{cases} 1 \\ \varphi_\sigma \varphi_\mu \\ \varphi_\sigma \varphi_\mu \end{cases}, \quad \tilde{\gamma}^{(b)} = \gamma \begin{cases} \varphi_\sigma \varphi_\mu \\ \varphi_\sigma \varphi_\mu \\ 1 \end{cases}, \quad \text{for} \begin{cases} r < R \\ R < r < R+e \\ r > R+e \end{cases}, \tag{2.15a}$$

$$\tilde{\gamma}^{(c)} = \gamma \begin{cases} 1 \\ \varphi_\sigma \varphi_\mu \\ \varphi_\sigma \varphi_\mu \\ 1 \end{cases}, \quad \text{for} \quad \begin{cases} r < R \\ R < r < R+e_1 \\ R+e_1 < r < R+e \\ r > R+e \end{cases}, \tag{2.15b}$$

and

$$D_k(X) = k^2 X - \frac{\partial}{\partial r}\left(\frac{1}{r}\frac{\partial}{\partial r}(rX)\right). \tag{2.16}$$

3. Boundary conditions and renormalization

3.1. *Boundary conditions*

The system of equations (2.14a, b) is completed by the appropriate boundary conditions for $r=0$ and $r\rightarrow\infty$,

$$B_r(r=0)=B_\theta(r=0)=\lim_{r\rightarrow\infty}B_r=\lim_{r\rightarrow\infty}B_\theta=0, \qquad (3.1a-d)$$

and by the continuity across $r=R$ and $r=R+e$ of the normal component of $\boldsymbol{B}$ and of the tangential components of $\boldsymbol{H}$ and $\boldsymbol{E}$,

$$[B_r]_{R^-}^{R^+}=[H_\theta]_{R^-}^{R^+}=[H_z]_{R^-}^{R^+}=[E_\theta]_{R^-}^{R^+}=[E_z]_{R^-}^{R^+}=0, \qquad (3.2a-e)$$

$$[B_r]_{(R+e)^-}^{(R+e)^+}=[H_\theta]_{(R+e)^-}^{(R+e)^+}=[H_z]_{(R+e)^-}^{(R+e)^+}=[E_\theta]_{(R+e)^-}^{(R+e)^+}=[E_z]_{(R+e)^-}^{(R+e)^+}=0, \qquad (3.3a-e)$$

and for case (c), by the continuity across $r=R+e_1$ of the same quantities,

$$[B_r]_{(R+e_1)^-}^{(R+e_1)^+}=[H_\theta]_{(R+e_1)^-}^{(R+e_1)^+}=[H_z]_{(R+e_1)^-}^{(R+e_1)^+}=[E_\theta]_{(R+e_1)^-}^{(R+e_1)^+}=[E_z]_{(R+e_1)^-}^{(R+e_1)^+}=0, \quad (3.4a-e)$$

where $[X]_{r_1}^{r_2}=X(r=r_2)-X(r=r_1)$.

From (2.9a) and (2.11b), the magnetic field $\boldsymbol{H}$ takes the form

$$\boldsymbol{H}=\left(\tilde{\varphi}_\mu\mu^\perp\right)^{-1}\begin{pmatrix}(1+\tilde{\mu}c^2)B_r+\tilde{\mu}csB_\theta\\ \tilde{\mu}csB_r+(1+\tilde{\mu}s^2)B_\theta\\ B_z\end{pmatrix}, \qquad (3.5)$$

with, from (2.9b),

$$B_z=\mathrm{i}k^{-1}(\frac{B_r}{r}+\frac{\partial B_r}{\partial r}). \qquad (3.6)$$

Then (3.2$a-c$) and (3.3$a-c$) can be rewritten, in case (a), as

$$B_r^{(a)}(R^+)=B_r^{(a)}(R^-) \qquad (3.7a)$$

$$\varphi_\mu^{-1}B_\theta^{(a)}(R^+)=\mu csB_r^{(a)}(R^-)+(1+\mu s^2)B_\theta^{(a)}(R^-) \qquad (3.7b)$$

$$\varphi_\mu^{-1}\left(\frac{B_r^{(a)}(R^+)}{R}+\frac{\partial B_r^{(a)}}{\partial r}(R^+)\right)=\frac{B_r^{(a)}(R^-)}{R}+\frac{\partial B_r^{(a)}}{\partial r}(R^-) \qquad (3.7c)$$

$$B_r^{(a)}((R+e)^-)=B_r^{(a)}((R+e)^+) \qquad (3.7d)$$

$$B_\theta^{(a)}((R+e)^-)=B_\theta^{(a)}((R+e)^+) \qquad (3.7e)$$

$$\frac{B_r^{(a)}((R+e)^-)}{(R+e)}+\frac{\partial B_r^{(a)}}{\partial r}((R+e)^-)=\frac{B_r^{(a)}((R+e)^+)}{(R+e)}+\frac{\partial B_r^{(a)}}{\partial r}((R+e)^+), \qquad (3.7f)$$

in case (b), as

$$B_r^{(b)}(R^+)=B_r^{(b)}(R^-) \qquad (3.8a)$$

$$B_\theta^{(b)}(R^+)=B_\theta^{(b)}(R^-) \qquad (3.8b)$$

$$\frac{B_r^{(b)}(R^+)}{R}+\frac{\partial B_r^{(b)}}{\partial r}(R^+)=\frac{B_r^{(b)}(R^-)}{R}+\frac{\partial B_r^{(b)}}{\partial r}(R^-) \qquad (3.8c)$$

$$B_r^{(b)}((R+e)^-)=B_r^{(b)}((R+e)^+) \qquad (3.8d)$$

$$\varphi_\mu^{-1}B_\theta^{(b)}((R+e)^-)=\mu csB_r^{(b)}((R+e)^+)+(1+\mu s^2)B_\theta^{(b)}((R+e)^+) \qquad (3.8e)$$

$$\varphi_\mu^{-1}\left(\frac{B_r^{(b)}((R+e)^-)}{(R+e)}+\frac{\partial B_r^{(b)}}{\partial r}((R+e)^-)\right)=\frac{B_r^{(b)}((R+e)^+)}{(R+e)}+\frac{\partial B_r^{(b)}}{\partial r}((R+e)^+). \quad (3.8f)$$

In case (c), $(3.2a-c)$, $(3.3a-c)$ and $(3.4a-c)$ can be rewritten as

$$B_r^{(c)}(R^+) = B_r^{(c)}(R^-) \tag{3.9a}$$

$$\varphi_\mu^{-1} B_\theta^{(c)}(R^+) = \mu c s B_r^{(c)}(R^-) + (1+\mu s^2) B_\theta^{(c)}(R^-) \tag{3.9b}$$

$$\varphi_\mu^{-1}\left(\frac{B_r^{(c)}(R^+)}{R} + \frac{\partial B_r^{(c)}}{\partial r}(R^+)\right) = \frac{B_r^{(c)}(R^-)}{R} + \frac{\partial B_r^{(c)}}{\partial r}(R^-) \tag{3.9c}$$

$$B_r^{(c)}((R+e_1)^+) = B_r^{(c)}((R+e_1)^-) \tag{3.9d}$$

$$B_\theta^{(c)}((R+e_1)^+) = B_\theta^{(c)}((R+e_1)^-) \tag{3.9e}$$

$$\frac{B_r^{(c)}((R+e_1)^+)}{R+e_1} + \frac{\partial B_r^{(c)}}{\partial r}((R+e_1)^+) = \frac{B_r^{(c)}((R+e_1)^-)}{R+e_1} + \frac{\partial B_r^{(c)}}{\partial r}((R+e_1)^-) \tag{3.9f}$$

$$B_r^{(c)}((R+e)^-) = B_r^{(c)}((R+e)^+) \tag{3.9g}$$

$$\varphi_\mu^{-1} B_\theta^{(c)}((R+e)^-) = \mu c s B_r^{(c)}((R+e)^+) + (1+\mu s^2) B_\theta^{(c)}((R+e)^+) \tag{3.9h}$$

$$\varphi_\mu^{-1}\left(\frac{B_r^{(c)}((R+e)^-)}{(R+e)} + \frac{\partial B_r^{(c)}}{\partial r}((R+e)^-)\right) = \frac{B_r^{(c)}((R+e)^+)}{(R+e)} + \frac{\partial B_r^{(c)}}{\partial r}((R+e)^+). \tag{3.9i}$$

From $(2.9d)$ we have $E_\theta = -\mathrm{i}k^{-1}\gamma B_r$, implying that the two conditions $(3.2a)$ and $(3.2d)$ are redundant, as are $(3.3a)$ and $(3.3d)$, and $(3.4a)$ and $(3.4d)$. As for the last boundary conditions $(3.2e)$, $(3.3e)$ and $(3.4e)$, using $(2.9e)$ we have

$$\tilde{\varphi}_\sigma^{-1} J_z + \sigma^\perp r \tilde{\Omega} B_r = \sigma^\perp E_z \tag{3.10}$$

with $\tilde{\Omega}$ defined in $(2.1a)$ and $(2.1b)$, leading to,
in case (a)

$$\varphi_\sigma^{-1} J_z^{(a)}(R^+) + \sigma^\perp \Omega R B_r^{(a)}(R^+) = J_z^{(a)}(R^-) + \sigma^\perp \Omega R B_r^{(a)}(R^-), \tag{3.11a}$$

$$\varphi_\sigma^{-1} J_z^{(a)}((R+e)^+) = \varphi_\sigma^{-1} J_z^{(a)}((R+e)^-) + \sigma^\perp \Omega (R+e) B_r^{(a)}((R+e)^-), \tag{3.11b}$$

in case (b)

$$\varphi_\sigma^{-1} J_z^{(b)}(R^+) = \varphi_\sigma^{-1} J_z^{(b)}(R^-) + \sigma^\perp \Omega R B_r^{(b)}(R^-), \tag{3.12a}$$

$$J_z^{(b)}((R+e)^+) = \varphi_\sigma^{-1} J_z^{(b)}((R+e)^-), \tag{3.12b}$$

and in case (c)

$$\varphi_\sigma^{-1} J_z^{(c)}(R^+) + \sigma^\perp \Omega R B_r^{(c)}(R^+) = J_z^{(c)}(R^-) + \sigma^\perp \Omega R B_r^{(c)}(R^-), \tag{3.13a}$$

$$\varphi_\sigma^{-1} J_z^{(c)}((R+e_1)^+) = \varphi_\sigma^{-1} J_z^{(c)}((R+e_1)^-) + \sigma^\perp \Omega (R+e_1) B_r^{(c)}((R+e_1)^-), \tag{3.13b}$$

$$J_z^{(c)}((R+e)^+) = \varphi_\sigma^{-1} J_z^{(c)}((R+e)^-). \tag{3.13c}$$

3.2. *Magnetic Reynolds number and renormalization*

By defining the magnetic Reynolds number in terms of the radius R, the angular velocity Ω, the electrical conductivity and magnetic permeability, $\sigma^\perp$ and $\mu^\perp$ in cases (a) and (c), and σ^F and μ^F in case (b), we obtain

$$Rm^{(a)} = \sigma^\perp \mu^\perp R^2 |\Omega^{(a)}|, \; Rm^{(b)} = \sigma^F \mu^F R^2 |\Omega^{(b)}|, \; Rm^{(c)} = \sigma^\perp \mu^\perp R^2 |\Omega^{(c)}|. \tag{3.14a-c}$$

Renormalizing the distance and time by R and $\sigma^\perp \mu^\perp R^2$, and the current density $\boldsymbol{J}$ by $(\mu^\perp R)^{-1}$, corresponds to replacing R, $\sigma^\perp$ and $\mu^\perp$ by unity in the system $(2.14a, b)$ and in the boundary conditions ($3.7a$-$3.13c$). Finally, for the sake of clarity, in sections 4, 5 and 6, the notations Ω, e and e_1 relate to dimensionless quantities . Then,

$$Rm^{(a)} = |\Omega^{(a)}|, \quad Rm^{(b)} = \varphi_\sigma \varphi_\mu |\Omega^{(b)}|, \quad Rm^{(c)} = |\Omega^{(c)}|. \tag{3.15a-c}$$

4. Solution

4.1. *Derivation of the differential equations satisfied by B_r and B_θ*

As we are interested in the dynamo threshold, the system (2.14a, b) is solved for $\gamma = 0$, taking the following form

$$D_k(B_r) = -\left[\tilde{\mu}c^2k^2B_r + \tilde{\sigma}s^2D_k(B_r) - cs(\tilde{\sigma}-\tilde{\mu})k^2B_\theta\right] \tag{4.1a}$$
$$D_k(B_\theta) = -\left[\tilde{\sigma}c^2k^2B_\theta + \tilde{\mu}s^2D_k(B_\theta) - cs(\tilde{\sigma}-\tilde{\mu})D_k(B_r)\right]. \tag{4.1b}$$

Considering the following linear combinations, c(4.1a)+s(4.1b) on the one hand, sD_k((4.1a))-ck^2(4.1b) on the other hand, leads to

$$(1+\tilde{\mu}s^2)D_k(cB_r + sB_\theta) = -\tilde{\mu}c^2k^2(cB_r + sB_\theta), \tag{4.2a}$$
$$(1+\tilde{\sigma}s^2)D_k(sD_k(B_r) - ck^2B_\theta) = -\tilde{\sigma}c^2k^2(sD_k(B_r) - ck^2B_\theta). \tag{4.2b}$$

Introducing

$$k_{\tilde{\sigma}} = k\left(\frac{1+\tilde{\sigma}}{1+\tilde{\sigma}s^2}\right)^{1/2}, \quad k_{\tilde{\mu}} = k\left(\frac{1+\tilde{\mu}}{1+\tilde{\mu}s^2}\right)^{1/2}, \tag{4.3a, b}$$

and with the help of the identity

$$D_{k_1}(X) = D_{k_2}(X) + (k_1^2 - k_2^2)X, \tag{4.4}$$

we can show that

$$(1+\tilde{\sigma}s^2)D_{k_{\tilde{\sigma}}}(X) = (1+\tilde{\sigma}s^2)D_k(X) + \tilde{\sigma}c^2k^2X, \tag{4.5a}$$
$$(1+\tilde{\mu}s^2)D_{k_{\tilde{\mu}}}(X) = (1+\tilde{\mu}s^2)D_k(X) + \tilde{\mu}c^2k^2X. \tag{4.5b}$$

Then, (4.2a) and (4.5b) on the one hand, (4.2b) and (4.5a) on the other hand, lead to

$$D_{k_{\tilde{\mu}}}(cB_r + sB_\theta) = 0, \tag{4.6a}$$
$$D_{k_{\tilde{\sigma}}}(sD_k(B_r) - ck^2B_\theta) = 0. \tag{4.6b}$$

Furthermore, from (4.1a) and (4.5a) on the one hand, from (4.1b) and (4.5b) on the other hand, we have

$$(1+\tilde{\sigma}s^2)D_{k_{\tilde{\sigma}}}(B_r) = (\tilde{\sigma}-\tilde{\mu})ck^2(cB_r + sB_\theta), \tag{4.7a}$$
$$(1+\tilde{\mu}s^2)D_{k_{\tilde{\mu}}}(B_\theta) = (\tilde{\sigma}-\tilde{\mu})c\left(sD_k(B_r) - ck^2B_\theta\right). \tag{4.7b}$$

Finally, using (4.6a, b) and (4.7a, b), leads to

$$\left(D_{k_{\tilde{\mu}}} \circ D_{k_{\tilde{\sigma}}}\right)(B_r) = \left(D_{k_{\tilde{\sigma}}} \circ D_{k_{\tilde{\mu}}}\right)(B_\theta) = 0. \tag{4.8a, b}$$

The two operators $D_{k_{\tilde{\sigma}}}$ and $D_{k_{\tilde{\mu}}}$ being commutative, B_r and B_θ satisfy the same linear differential equation of fourth order.

4.2. *General expressions of B_r and B_θ*

As the solution of $D_\nu(X) = 0$ is a linear combination of $I_1(\nu r)$ and $K_1(\nu r)$, where I_1 and K_1 are first and second kind modified Bessel functions of order 1, the solutions of (4.8a, b) are a linear combination of $I_1(k_{\tilde{\sigma}}r)$, $K_1(k_{\tilde{\sigma}}r)$, $I_1(k_{\tilde{\mu}}r)$ and $K_1(k_{\tilde{\mu}}r)$. Applying the boundary conditions (3.1$a-d$), B_r and B_θ can be written in the following form, in case (a)

$$B_r^{(a)} = \begin{cases} r<1, & -s\left(\lambda_\sigma^R \dfrac{I_1(k_\sigma r)}{I_1(k_\sigma)} + \lambda_\mu^R \dfrac{I_1(k_\mu r)}{I_1(k_\mu)}\right) \\ 1<r<1+e & -s\left(\lambda_r^I \dfrac{I_1(kr)}{I_1(k)} + \lambda_r^K \dfrac{K_1(kr)}{K_1(k)}\right) \\ r>1+e, & -s\lambda_r^S \dfrac{K_1(kr)}{K_1(k(1+e))} \end{cases}, \tag{4.9}$$

$$B_\theta^{(a)} = \begin{cases} r<1, & c\left(\lambda_\sigma^R \dfrac{I_1(k_\sigma r)}{I_1(k_\sigma)} + \dfrac{\mu s^2}{1+\mu s^2}\lambda_\mu^R \dfrac{I_1(k_\mu r)}{I_1(k_\mu)}\right) \\ 1<r<1+e, & c\left(\lambda_\theta^I \dfrac{I_1(kr)}{I_1(k)} + \lambda_\theta^K \dfrac{K_1(kr)}{K_1(k)}\right) \\ r>1+e, & c\lambda_\theta^S \dfrac{K_1(kr)}{K_1(k(1+e))} \end{cases}, \tag{4.10}$$

where (4.10a) has been obtained by replacing (4.9a) in (4.7a), and where (4.9b,c) and (4.10b,c) result from $D_k(B_r) = D_k(B_\theta) = 0$ for $r > 1$.

In case (b),

$$B_r^{(b)} = \begin{cases} r<1, & -s\lambda_r^R \dfrac{I_1(kr)}{I_1(k)} \\ 1<r<1+e & -s\left(\lambda_r^I \dfrac{I_1(kr)}{I_1(k)} + \lambda_r^K \dfrac{K_1(kr)}{K_1(k)}\right) \\ r>1+e, & -s\left(\lambda_\sigma^S \dfrac{K_1(k_\sigma r)}{K_1(k_\sigma(1+e))} + \lambda_\mu^S \dfrac{K_1(k_\mu r)}{K_1(k_\mu(1+e))}\right) \end{cases}, \tag{4.11}$$

$$B_\theta^{(b)} = \begin{cases} r<1, & c\lambda_\theta^R \dfrac{I_1(kr)}{I_1(k)} \\ 1<r<1+e, & c\left(\lambda_\theta^I \dfrac{I_1(kr)}{I_1(k)} + \lambda_\theta^K \dfrac{K_1(kr)}{K_1(k)}\right) \\ r>1+e, & c\left(\lambda_\sigma^S \dfrac{K_1(k_\sigma r)}{K_1(k_\sigma(1+e))} + \dfrac{\mu s^2}{1+\mu s^2}\lambda_\mu^S \dfrac{K_1(k_\mu r)}{K_1(k_\mu(1+e))}\right) \end{cases}, \tag{4.12}$$

where (4.12c) has been obtained by replacing (4.11c) in (4.7a), and where (4.11a,b) and (4.12a,b) result from $D_k(B_r) = D_k(B_\theta) = 0$ for $r < 1+e$.

In case (c),

$$B_r^{(c)} = \begin{cases} r<1, & -s\left(\lambda_\sigma^R \dfrac{I_1(k_\sigma r)}{I_1(k_\sigma)} + \lambda_\mu^R \dfrac{I_1(k_\mu r)}{I_1(k_\mu)}\right) \\ 1<r<1+e_1, & -s\left(\lambda_{r_1}^I \dfrac{I_1(kr)}{I_1(k)} + \lambda_{r_1}^K \dfrac{K_1(kr)}{K_1(k)}\right) \\ 1+e_1<r<1+e, & -s\left(\lambda_{r_2}^I \dfrac{I_1(kr)}{I_1(k(1+e_1))} + \lambda_{r_2}^K \dfrac{K_1(kr)}{K_1(k(1+e_1))}\right) \\ r>1+e, & -s\left(\lambda_\sigma^S \dfrac{K_1(k_\sigma r)}{K_1(k_\sigma(1+e))} + \lambda_\mu^S \dfrac{K_1(k_\mu r)}{K_1(k_\mu(1+e))}\right) \end{cases}, \tag{4.13}$$

$$B_\theta^{(c)} = \begin{cases} r<1,\ c\left(\lambda_\sigma^R \dfrac{I_1(k_\sigma r)}{I_1(k_\sigma)} + \dfrac{\mu s^2}{1+\mu s^2}\lambda_\mu^R \dfrac{I_1(k_\mu r)}{I_1(k_\mu)}\right) \\ 1<r<1+e_1,\ c\left(\lambda_{\theta_1}^I \dfrac{I_1(kr)}{I_1(k)} + \lambda_{\theta_1}^K \dfrac{K_1(kr)}{K_1(k)}\right) \\ 1+e_1<r<1+e,\ c\left(\lambda_{\theta_2}^I \dfrac{I_1(kr)}{I_1(k(1+e_1))} + \lambda_{\theta_2}^K \dfrac{K_1(kr)}{K_1(k(1+e_1))}\right) \\ r>1+e,\ c\left(\lambda_\sigma^S \dfrac{K_1(k_\sigma r)}{K_1(k_\sigma(1+e))} + \dfrac{\mu s^2}{1+\mu s^2}\lambda_\mu^S \dfrac{K_1(k_\mu r)}{K_1(k_\mu(1+e))}\right) \end{cases} ,(4.14)$$

where (4.14a) and (4.14d) have been obtained by replacing (4.13a) and (4.13d) in (4.7a), and where (4.13b,c) and (4.14b,c) result from $D_k(B_r) = D_k(B_\theta) = 0$ for $1 < r < 1+e$.

4.3. *Application of other boundary conditions*

From (4.9-4.10) in case (a), and (4.11-4.12) in case (b), there are eight unknowns, $(\lambda^R_{\sigma,\mu}, \lambda^{I,K}_r, \lambda^{I,K}_\theta, \lambda^S_{r,\theta})$ in case (a), and $(\lambda^R_{r,\theta}, \lambda^{I,K}_r, \lambda^{I,K}_\theta, \lambda^S_{\sigma,\mu})$ in case (b). Therefore, each problem needs eight equations to be solved. In case (c), from (4.13-4.14), there are twelve unknowns, $(\lambda^R_{\sigma,\mu}, \lambda^{I,K}_{r_1}, \lambda^{I,K}_{\theta_1}, \lambda^{I,K}_{r_2}, \lambda^{I,K}_{\theta_2}, \lambda^S_{\sigma,\mu})$, needing twelve equations to be solved.

In case (a), the six first equations are given by the boundary conditions (3.7$a-f$), leading to

$$\lambda_r^I + \lambda_r^K = \lambda_\sigma^R + \lambda_\mu^R, \tag{4.15a}$$
$$\varphi_\mu^{-1}\left(\lambda_\theta^I + \lambda_\theta^K\right) = \lambda_\sigma^R, \tag{4.15b}$$
$$-k\varphi_\mu^{-1}\left(-\lambda_r^I \tfrac{I_0(k)}{I_1(k)} + \lambda_r^K \tfrac{K_0(k)}{K_1(k)}\right) = k_\sigma \lambda_\sigma^R \tfrac{I_0(k_\sigma)}{I_1(k_\sigma)} + k_\mu \lambda_\mu^R \tfrac{I_0(k_\mu)}{I_1(k_\mu)}, \tag{4.15c}$$
$$\lambda_r^I \tfrac{I_1(k(1+e))}{I_1(k)} + \lambda_r^K \tfrac{K_1(k(1+e))}{K_1(k)} = \lambda_r^S, \tag{4.15d}$$
$$\lambda_\theta^I \tfrac{I_1(k(1+e))}{I_1(k)} + \lambda_\theta^K \tfrac{K_1(k(1+e))}{K_1(k)} = \lambda_\theta^S, \tag{4.15e}$$
$$-\lambda_r^I \tfrac{I_0(k(1+e))}{I_1(k)} + \lambda_r^K \tfrac{K_0(k(1+e))}{K_1(k)} = \lambda_r^S \tfrac{K_0(k(1+e))}{K_1(k(1+e))}. \tag{4.15f}$$

In case (b) they are given by the boundary conditions (3.8$a-f$), leading to

$$\lambda_r^I + \lambda_r^K = \lambda_r^R, \tag{4.16a}$$
$$\lambda_\theta^I + \lambda_\theta^K = \lambda_\theta^R, \tag{4.16b}$$
$$\lambda_r^I \tfrac{I_0(k)}{I_1(k)} - \lambda_r^K \tfrac{K_0(k)}{K_1(k)} = \lambda_r^R \tfrac{I_0(k)}{I_1(k)}, \tag{4.16c}$$
$$\lambda_r^I \tfrac{I_1(k(1+e))}{I_1(k)} + \lambda_r^K \tfrac{K_1(k(1+e))}{K_1(k)} = \lambda_\sigma^S + \lambda_\mu^S, \tag{4.16d}$$
$$\varphi_\mu^{-1}\left(\lambda_\theta^I \tfrac{I_1(k(1+e))}{I_1(k)} + \lambda_\theta^K \tfrac{K_1(k(1+e))}{K_1(k)}\right) = \lambda_\sigma^S, \tag{4.16e}$$
$$k\varphi_\mu^{-1}\left(-\lambda_r^I \tfrac{I_0(k(1+e))}{I_1(k)} + \lambda_r^K \tfrac{K_0(k(1+e))}{K_1(k)}\right) = k_\sigma \lambda_\sigma^S \tfrac{K_0(k_\sigma(1+e))}{K_1(k_\sigma(1+e))} + k_\mu \lambda_\mu^S \tfrac{K_0(k_\mu(1+e))}{K_1(k_\mu(1+e))}. \tag{4.16f}$$

In case (c), the nine first equations are given by the boundary conditions (3.9$a-i$), leading to

$$\lambda^I_{r_1} + \lambda^K_{r_1} = \lambda^R_\sigma + \lambda^R_\mu, \tag{4.17a}$$

$$\varphi_\mu^{-1}\left(\lambda^I_{\theta_1} + \lambda^K_{\theta_1}\right) = \lambda^R_\sigma, \tag{4.17b}$$

$$-k\varphi_\mu^{-1}\left(-\lambda^I_{r_1}\tfrac{I_0(k)}{I_1(k)} + \lambda^K_{r_1}\tfrac{K_0(k)}{K_1(k)}\right) = k_\sigma\lambda^R_\sigma\tfrac{I_0(k_\sigma)}{I_1(k_\sigma)} + k_\mu\lambda^R_\mu\tfrac{I_0(k_\mu)}{I_1(k_\mu)}, \tag{4.17c}$$

$$\lambda^I_{r_1}\tfrac{I_1(k(1+e_1))}{I_1(k)} + \lambda^K_{r_1}\tfrac{K_1(k(1+e_1))}{K_1(k)} = \lambda^I_{r_2} + \lambda^K_{r_2}, \tag{4.17d}$$

$$\lambda^I_{\theta_1}\tfrac{I_1(k(1+e_1))}{I_1(k)} + \lambda^K_{\theta_1}\tfrac{K_1(k(1+e_1))}{K_1(k)} = \lambda^I_{\theta_2} + \lambda^K_{\theta_2}, \tag{4.17e}$$

$$-\lambda^I_{r_1}\tfrac{I_0(k(1+e_1))}{I_1(k)} + \lambda^K_{r_1}\tfrac{K_0(k(1+e_1))}{K_1(k)} = -\lambda^I_{r_2}\tfrac{I_0(k(1+e_1))}{I_1(k(1+e_1))} + \lambda^K_{r_2}\tfrac{K_0(k(1+e_1))}{K_1(k(1+e_1))}, \tag{4.17f}$$

$$\lambda^I_{r_2}\tfrac{I_1(k(1+e))}{I_1(k(1+e_1))} + \lambda^K_{r_2}\tfrac{K_1(k(1+e))}{K_1(k(1+e_1))} = \lambda^S_\sigma + \lambda^S_\mu, \tag{4.17g}$$

$$\varphi_\mu^{-1}\left(\lambda^I_{\theta_2}\tfrac{I_1(k(1+e))}{I_1(k(1+e_1))} + \lambda^K_{\theta_2}\tfrac{K_1(k(1+e))}{K_1(k(1+e_1))}\right) = \lambda^S_\sigma, \tag{4.17h}$$

$$k\varphi_\mu^{-1}\left(-\lambda^I_{r_2}\tfrac{I_0(k(1+e))}{I_1(k(1+e_1))} + \lambda^K_{r_2}\tfrac{K_0(k(1+e))}{K_1(k(1+e_1))}\right) = k_\sigma\lambda^S_\sigma\tfrac{K_0(k_\sigma(1+e))}{K_1(k_\sigma(1+e))} + k_\mu\lambda^S_\mu\tfrac{K_0(k_\mu(1+e))}{K_1(k_\mu(1+e))}. \tag{4.17i}$$

Finally, to apply the last boundary conditions $(3.11a,b)$ in case (a), $(3.12a,b)$ in case (b), $(3.13a-c)$ in case (c), we need to calculate the z-component of the current density, that is given by

$$J_z = \tilde{\varphi}_\mu^{-1}\frac{1}{r}\frac{\partial}{\partial r}(r\tilde{\phi}), \text{ with } \tilde{\phi} = \tilde{\mu}csB_r + (1+\tilde{\mu}s^2)B_\theta. \tag{4.18a, b}$$

In case (a), replacing $B_r^{(a)}$ and $B_\theta^{(a)}$ given by (4.9) and (4.10), in (4.18b) leads to

$$\tilde{\phi}^{(a)} = \begin{cases} r<1, & c\lambda^R_\sigma\dfrac{I_1(k_\sigma r)}{I_1(k_\sigma)} \\ 1<r<1+e, & c\left(\lambda^I_\theta\dfrac{I_1(kr)}{I_1(k)} + \lambda^K_\theta\dfrac{K_1(kr)}{K_1(k)}\right) \\ r>1+e, & c\lambda^S_\theta\dfrac{K_1(kr)}{K_1(k(1+e))} \end{cases}. \tag{4.19}$$

In case (b), replacing $B_r^{(b)}$ and $B_\theta^{(b)}$ given by (4.11) and (4.12), in (4.18b) leads to

$$\tilde{\phi}^{(b)} = \begin{cases} r<1, & c\lambda^R_\theta\dfrac{I_1(kr)}{I_1(k)} \\ 1<r<1+e, & c\left(\lambda^I_\theta\dfrac{I_1(kr)}{I_1(k)} + \lambda^K_\theta\dfrac{K_1(kr)}{K_1(k)}\right) \\ r>1+e, & c\lambda^S_\sigma\dfrac{K_1(k_\sigma r)}{K_1(k_\sigma(1+e))} \end{cases}. \tag{4.20}$$

In case (c), replacing $B_r^{(c)}$ and $B_\theta^{(c)}$ given by (4.13) and (4.14), in (4.18b) leads to

$$\tilde{\phi}^{(c)} = \begin{cases} r<1, & c\lambda_\sigma^R \dfrac{I_1(k_\sigma r)}{I_1(k_\sigma)} \\ 1<r<1+e_1, & c\left(\lambda_{\theta_1}^I \dfrac{I_1(kr)}{I_1(k)} + \lambda_{\theta_1}^K \dfrac{K_1(kr)}{K_1(k)}\right) \\ 1+e_1<r<1+e, & c\left(\lambda_{\theta_2}^I \dfrac{I_1(kr)}{I_1(k)} + \lambda_{\theta_2}^K \dfrac{K_1(kr)}{K_1(k)}\right) \\ r>1+e, & c\lambda_\sigma^S \dfrac{K_1(k_\sigma r)}{K_1(k_\sigma(1+e))} \end{cases}. \tag{4.21}$$

Applying the relations $\partial_r(rI_1(\nu r)) = \nu r I_0(\nu r)$ and $\partial_r(rK_1(\nu r)) = -\nu r K_0(\nu r)$, where ν is a dummy variable, to (4.18a), leads to,
in case (a),

$$J_z^{(a)} = \begin{cases} r<1, & ck_\sigma \lambda_\sigma^R \dfrac{I_0(k_\sigma r)}{I_1(k_\sigma)} \\ 1<r<1+e, & ck\varphi_\mu^{-1}\left(\lambda_\theta^I \dfrac{I_0(kr)}{I_1(k)} - \lambda_\theta^K \dfrac{K_0(kr)}{K_1(k)}\right) \\ r>1+e, & -ck\varphi_\mu^{-1}\lambda_\theta^S \dfrac{K_0(kr)}{K_1(k(1+e))} \end{cases}, \tag{4.22}$$

in case (b),

$$J_z^{(b)} = \begin{cases} r<1, & ck\varphi_\mu^{-1} \lambda_\theta^R \dfrac{I_0(kr)}{I_1(k)} \\ 1<r<1+e, & ck\varphi_\mu^{-1}\left(\lambda_\theta^I \dfrac{I_0(kr)}{I_1(k)} - \lambda_\theta^K \dfrac{K_0(kr)}{K_1(k)}\right) \\ r>1+e, & -ck_\sigma\lambda_\sigma^S \dfrac{K_0(k_\sigma r)}{K_1(k_\sigma(1+e))} \end{cases}, \tag{4.23}$$

in case (c),

$$J_z^{(c)} = \begin{cases} r<1, & ck_\sigma \lambda_\sigma^R \dfrac{I_0(k_\sigma r)}{I_1(k_\sigma)} \\ 1<r<1+e_1, & ck\varphi_\mu^{-1}\left(\lambda_{\theta_1}^I \dfrac{I_0(kr)}{I_1(k)} - \lambda_{\theta_1}^K \dfrac{K_0(kr)}{K_1(k)}\right) \\ 1+e_1<r<1+e, & ck\varphi_\mu^{-1}\left(\lambda_{\theta_2}^I \dfrac{I_0(kr)}{I_1(k(1+e_1))} - \lambda_{\theta_2}^K \dfrac{K_0(kr)}{K_1(k(1+e_1))}\right) \\ r>1+e, & -ck_\sigma\lambda_\sigma^S \dfrac{K_0(k_\sigma r)}{K_1(k_\sigma(1+e))} \end{cases}. \tag{4.24}$$

In case (a), replacing (4.9) and (4.22) in $(3.11a,b)$, leads to

$$\varphi_\sigma^{-1}\varphi_\mu^{-1}ck\left(\lambda_\theta^I \tfrac{I_0(k)}{I_1(k)} - \lambda_\theta^K \tfrac{K_0(k)}{K_1(k)}\right) - \varOmega s(\lambda_r^I + \lambda_r^K) = ck_\sigma\lambda_\sigma^R \tfrac{I_0(k_\sigma)}{I_1(k_\sigma)} - \varOmega s\left(\lambda_\sigma^R + \lambda_\mu^R\right), \tag{4.25a}$$

$$\varphi_\sigma^{-1}\varphi_\mu^{-1}ck\left(\lambda_\theta^I \tfrac{I_0(k(1+e))}{I_1(k)} - \lambda_\theta^K \tfrac{K_0(k(1+e))}{K_1(k)}\right) - \varOmega s(1+e)\left(\lambda_r^I \tfrac{I_1(k(1+e))}{I_1(k)} + \lambda_r^K \tfrac{K_1(k(1+e))}{K_1(k)}\right) = -\varphi_\sigma^{-1}\varphi_\mu^{-1}ck\lambda_\theta^S \tfrac{K_0(k(1+e))}{K_1(k(1+e))}. \tag{4.25b}$$

In case (b), replacing (4.11) and (4.23) in (3.12a, b), leads to

$$\varphi_\sigma^{-1}\varphi_\mu^{-1}ck\left(\lambda_\theta^I\frac{I_0(k)}{I_1(k)}-\lambda_\theta^K\frac{K_0(k)}{K_1(k)}\right)=\varphi_\sigma^{-1}\varphi_\mu^{-1}ck\lambda_\theta^R\frac{I_0(k)}{I_1(k)}-\Omega s\lambda_r^R \tag{4.26a}$$

$$\varphi_\sigma^{-1}\varphi_\mu^{-1}ck\left(\lambda_\theta^I\frac{I_0(k(1+e))}{I_1(k)}-\lambda_\theta^K\frac{K_0(k(1+e))}{K_1(k)}\right)=-ck_\sigma\lambda_\sigma^S\frac{K_0(k_\sigma(1+e))}{K_1(k_\sigma(1+e))}. \tag{4.26b}$$

In case (c), replacing (4.13) and (4.24) in (3.13a, c), leads to

$$\begin{aligned}\varphi_\sigma^{-1}\varphi_\mu^{-1}ck\left(\lambda_{\theta_1}^I\frac{I_0(k)}{I_1(k)}-\lambda_{\theta_1}^K\frac{K_0(k)}{K_1(k)}\right)-\Omega s(\lambda_{r_1}^I+\lambda_{r_1}^K)&\\ =ck_\sigma\lambda_\sigma^R\frac{I_0(k_\sigma)}{I_1(k_\sigma)}-\Omega s\left(\lambda_\sigma^R+\lambda_\mu^R\right)&\end{aligned} \tag{4.27a}$$

$$\begin{aligned}&\varphi_\sigma^{-1}\varphi_\mu^{-1}ck\left(\lambda_{\theta_1}^I\frac{I_0(k(1+e_1))}{I_1(k)}-\lambda_{\theta_1}^K\frac{K_0(k(1+e_1))}{K_1(k)}\right)\\ &-\Omega s(1+e_1)\left(\lambda_{r_1}^I\frac{I_1(k(1+e_1))}{I_1(k)}+\lambda_{r_1}^K\frac{K_1(k(1+e_1))}{K_1(k)}\right)\\ &=\varphi_\sigma^{-1}\varphi_\mu^{-1}ck\left(\lambda_{\theta_2}^I\frac{I_0(k(1+e_1))}{I_1(k(1+e_1))}-\lambda_{\theta_2}^K\frac{K_0(k(1+e_1))}{K_1(k(1+e_1))}\right)\end{aligned} \tag{4.27b}$$

$$\varphi_\sigma^{-1}\varphi_\mu^{-1}ck\left(\lambda_{\theta_2}^I\frac{I_0(k(1+e))}{I_1(k(1+e_1))}-\lambda_{\theta_2}^K\frac{K_0(k(1+e))}{K_1(k(1+e_1))}\right)=-ck_\sigma\lambda_\sigma^S\frac{K_0(k_\sigma(1+e))}{K_1(k_\sigma(1+e))}. \tag{4.27c}$$

5. Dynamo thresholds

In each case (a), (b) and (c), a dispersion relation can be derived, writing that the system composed of the eight equations (4.15$a-f$) and (4.25a, b) in case (a), (4.16$a-f$) and (4.26a, b) in case (b), or twelve equations (4.17$a-i$) and (4.27$a-c$) in case (c), is singular (zero determinant). Their derivations (see Appendices B, C and D) lead to the following dynamo thresholds,
in case (a)

$$\Omega^{(a)}=-\frac{c}{s}\frac{1}{(1+e)^2\beta'^2}\frac{B(\sigma)B(\mu)}{E_{\sigma\mu}}, \tag{5.1}$$

in case (b),

$$\Omega^{(b)}=-\frac{c}{s}\alpha'^2\frac{C(\sigma)C(\mu)}{F_{\sigma\mu}}, \tag{5.2}$$

in case (c),

$$\Omega^{(c)}=-\frac{c}{s}\frac{1}{(1+e_1)^2}\frac{P(\sigma)P(\mu)}{E_{\sigma\mu}Q(\sigma)Q(\mu)+F_{\sigma\mu}R(\sigma)R(\mu)}, \tag{5.3}$$

with

$$(k',k'_\sigma,k'_\mu)=(1+e)(k,k_\sigma,k_\mu),\quad k_\sigma=k\left(\frac{1+\sigma}{1+\sigma s^2}\right)^{1/2},\quad k_\mu=k\left(\frac{1+\mu}{1+\mu s^2}\right)^{1/2}, \tag{5.4a}$$

$$k_1=(1+e_1)k,\quad \Phi(x)=x\frac{I_0(x)}{I_1(x)},\quad \Psi(x)=x\frac{K_0(x)}{K_1(x)}, \tag{5.4b}$$

$$\alpha_1=\frac{I_1(k_1)}{I_1(k)},\quad \beta_1=\frac{K_1(k_1)}{K_1(k)},\quad \alpha'=\frac{I_1(k')}{I_1(k)},\quad \beta'=\frac{K_1(k')}{K_1(k)},\quad \alpha=\frac{\alpha'}{\alpha_1},\quad \beta=\frac{\beta'}{\beta_1}, \tag{5.4c}$$

$$A(\nu)=\Phi(k_\nu)-\varphi_\nu^{-1}\Phi(k),\ B(\nu)=\Phi(k_\nu)+\varphi_\nu^{-1}\Psi(k),\ C(\nu)=\Psi(k'_\nu)+\varphi_\nu^{-1}\Phi(k'), \tag{5.4d}$$

$$D(\nu)=\Psi(k'_\nu)-\varphi_\nu^{-1}\Psi(k'),\ E_{\sigma\mu}=\Phi(k_\sigma)-\Phi(k_\mu),\ F_{\sigma\mu}=\Psi(k'_\sigma)-\Psi(k'_\mu), \tag{5.4e}$$

$$P(\nu)=\frac{\beta}{\alpha_1}A(\nu)D(\nu)-\frac{\alpha}{\beta_1}B(\nu)C(\nu),\ Q(\nu)=\alpha C(\nu)-\beta D(\nu),\ R(\nu)=\frac{A(\nu)}{\alpha_1}-\frac{B(\nu)}{\beta_1} \tag{5.4f}$$

where ν is a dummy variable which is equal to either σ or μ. We note that $A(\nu), B(\nu), C(\nu)$ and $D(\nu)$ are related to each other (see (A 4) in Appendix A). As mentioned in section 2.3 and in agreement with previous works (Favier & Proctor 2013; Marcotte *et al.* 2021), according to (5.1-5.3), the dynamo threshold remains unchanged when swapping σ and μ, φ_σ and φ_μ, Ω and $-\Omega$.

For $e \neq 0$ in cases (a) and (b), for $e_1 \neq 0$ and $e > e_1$ in case (c), (5.1-5.3) demonstrate the existence a remote effect of electrical conductivity anisotropy or magnetic permeability anisotropy on dynamo action. Of course, and as mentioned earlier, we expect this effect to disappear asymptotically in the limit $e \gg 1$ in cases (a) and (b), in the limit $e \gg e_1 \gg 1$ in case (c). In cases (a) and (b) for $e \gg 1$, we have $k' \gg 1$, $k'_\mu \gg 1$ and $k'_\sigma \gg 1$. Knowing that for $x \gg 1$, $I_0(x) \equiv I_1(x) \approx \exp(x)/\sqrt{2\pi x} \to \infty$ and $K_0(x) \equiv K_1(x) \approx e^{-x}\sqrt{\pi/2x} \to 0$, replacing in (5.1) and (5.2), we find that

$$\text{for e} \gg 1, \quad \Omega^{(a)} \propto e^{-1}\exp(2ke) \gg 1 \quad \text{and} \quad \Omega^{(b)} \propto \exp(2ke) \gg 1. \tag{5.5}$$

In case (c) for $e \gg e_1 \gg 1$, the asymptotic attenuation of the remote effect will become evident from the result of section 6.2 in which it is shown that the case (c) with $e \gg 1$ corresponds to the case (a) in which e must be replaced by e_1.

6. Checks

At this stage, we can perform several checks to verify consistency with previously published results, but also between case (c) and case (a) or case (b). We will show that

- Cases (a) and (b) for $e = 0$ can be retrieved from Plunian & Alboussière (2023).
- Case (a) can be retrieved from case (c) by taking in case (c), $e \gg 1$ and where e_1 corresponds to e of case (a).
- Case (b) can be retrieved from case (c) by taking in case (c), $e_1 \gg 1$, $e = O(e_1)$, and where the dimensionless radius $1 + e_1$ of case (c) corresponds to a radius equal to unity in case (b) and where the gap $e - e_1$ of case (c) corresponds to e of case (b).
- Case (c) for $e = 0$ can be retrieved from Plunian & Alboussière (2021).
- Case (c) for $e_1 = 0$ can be retrieved from Plunian *et al.* (2025).
- Case (c) for $e_1 = e$ can be retrieved from Plunian *et al.* (2025).

6.1. *Cases (a) and (b) for* $e = 0$

Taking $e = 0$ implies that $(k', k'_\sigma, k'_\mu) = (k, k_\sigma, k_\mu)$ and $\alpha' = \beta' = 1$. Then, the dispersion relations (5.1) and (5.2) take the following form,

$$\Omega^{(a)}_{e=0} = -\frac{c}{s}\frac{(\varphi_\sigma^{-1}\Psi(k) + \Phi(k_\sigma))(\varphi_\mu^{-1}\Psi(k) + \Phi(k_\mu))}{\Phi(k_\sigma) - \Phi(k_\mu)}, \tag{6.1}$$

and

$$\Omega^{(b)}_{e=0} = -\frac{c}{s}\frac{(\varphi_\sigma^{-1}\Phi(k) + \Psi(k_\sigma))(\varphi_\mu^{-1}\Phi(k) + \Psi(k_\mu))}{\Psi(k_\sigma) - \Psi(k_\mu)}. \tag{6.2}$$

In Plunian & Alboussière (2023) the dynamo threshold has been derived in the form

$$\Omega_{2023} = -\frac{c}{s}\frac{\left(\Phi(k_{\sigma_{\text{in}}}) + \overline{\varphi}_\sigma^{-1}\Psi(k_{\sigma_{\text{out}}})\right)\left(\Phi(k_{\mu_{\text{in}}}) + \overline{\varphi}_\mu^{-1}\Psi(k_{\mu_{\text{out}}})\right)}{\Phi(k_{\sigma_{\text{in}}}) + \Psi(k_{\sigma_{\text{out}}}) - \Phi(k_{\mu_{\text{in}}}) - \Psi(k_{\mu_{\text{out}}})}, \tag{6.3}$$

where the subscripts "in" and "out" correspond to $r < R$ and $r > R$ respectively, Ω_{2023} denotes the rotor velocity normalized by $R^2\sigma^\perp_{\text{in}}\mu^\perp_{\text{in}}$, $\overline{\varphi}_\sigma = \sigma^\perp_{\text{out}}/\sigma^\perp_{\text{in}}$ and $\overline{\varphi}_\mu = \mu^\perp_{\text{out}}/\mu^\perp_{\text{in}}$.
In case (a), $(\sigma_{\text{in}}, \mu_{\text{in}}) = (\sigma, \mu)$ and $(\sigma_{\text{out}}, \mu_{\text{out}}) = (0, 0)$, implying that $\overline{\varphi}_\sigma = \varphi_\sigma$ and $\overline{\varphi}_\mu = \varphi_\mu$. Then, $\Omega^{(a)}_{e=0}$ that is given in (6.1), corresponds directly to Ω_{2023} in (6.3), with $k_{\sigma_{\text{in}}} = k_\sigma$, $k_{\mu_{\text{in}}} = k_\mu$, and $k_{\sigma_{\text{out}}} = k_{\mu_{\text{out}}} = k$.
In case (b), as already mentioned in (3.15*b*), $|\Omega^{(b)}_{e=0}|$ must be multiplied by $\varphi_\sigma\varphi_\mu$ to obtain

the magnetic Reynolds number $Rm^{(b)}$. In addition, $(\sigma_{\text{in}}, \mu_{\text{in}}) = (0, 0)$ and $(\sigma_{\text{out}}, \mu_{\text{out}}) = (\sigma, \mu)$, implying that $\overline{\varphi}_\sigma = \varphi_\sigma^{-1}$ and $\overline{\varphi}_\mu = \varphi_\mu^{-1}$. Therefore, the expression of $\Omega^{(b)}_{e=0}$ given in (6.2), corresponds to $\varphi_\sigma^{-1}\varphi_\mu^{-1}\Omega_{2023}$ in (6.3), with $k_{\sigma_{\text{in}}} = k_{\mu_{\text{in}}} = k$, $k_{\sigma_{\text{out}}} = k_\sigma$ and $k_{\mu_{\text{out}}} = k_\mu$.

6.2. *Case (c) for $e \gg 1$*

In the asymptotic limit $e \gg 1$, we have $(k', k'_\mu, k'_\sigma) = O(e)$ and $(k, k_1) = O(1)$. In addition, we know that for $x \gg 1$, $(I_0(x), I_1(x)) \propto \exp(x)/\sqrt{x}$ and $(K_0(x), K_1(x)) \propto \exp(-x)/\sqrt{x}$ (Abramowitz & Stegun 1968). Then, we have $(\alpha, \alpha') \propto \exp(e)/\sqrt{e}$, $(\beta, \beta') \propto \exp(-e)/\sqrt{e}$, and $(\alpha_1, \beta_1) = O(1)$, implying $(A(\nu), B(\nu), E_{\sigma\mu}) = O(1)$ and $(C(\nu), D(\nu), F_{\sigma\mu}) = O(e)$. Then $P(\nu) \approx -\frac{\alpha}{\beta_1}B(\nu)C(\nu)$, $Q(\nu) \approx \alpha C(\nu)$ and $E_{\sigma\mu}Q(\sigma)Q(\mu) \gg F_{\sigma\mu}R(\sigma)R(\mu)$. Replacing in (5.3) then leads to (5.1) in which e must be replaced by e_1. Therefore case (c) with $e \gg 1$ corresponds to case (a).

6.3. *Case (c) for $e_1 \gg 1$ and $e = O(e_1)$*

In the asymptotic limit $e_1 \gg 1$ and $e = O(e_1)$, we have $(k_1, k', k'_\mu, k'_\sigma) = O(e_1)$ and $k = O(1)$. As written above, we know that for $x \gg 1$, $(I_0(x), I_1(x)) \propto \exp(x)/\sqrt{x}$ and $(K_0(x), K_1(x)) \propto \exp(-x)/\sqrt{x}$ (Abramowitz & Stegun 1968). Then, we have $(\alpha_1, \alpha') \propto \exp(e_1)/\sqrt{e_1}$, $(\beta_1, \beta') \propto \exp(-e_1)/\sqrt{e_1}$, and $(\alpha, \beta) = O(1)$. Then we have $(A(\nu), B(\nu), E_{\sigma\mu}) = O(1)$ and $(C(\nu), D(\nu), F_{\sigma\mu}) = O(e_1)$, implying that $P(\nu) \approx -\frac{\alpha}{\beta_1}B(\nu)C(\nu)$, $Q(\nu) = O(e_1)$, $R(\nu) \approx -B(\nu)/\beta_1$ and $F_{\sigma\mu}R(\sigma)R(\mu) \gg E_{\sigma\mu}Q(\sigma)Q(\mu)$. Replacing in (5.3) then leads to

$$\Omega^{(c)} \approx -\frac{c}{s}\frac{\alpha^2}{(1+e_1)^2}\frac{C(\sigma)C(\mu)}{F_{\sigma\mu}}. \tag{6.4}$$

In order to compare (6.4) to the dynamo threshold (5.2) of case (b), we must take into account that the rotor of dimensionless radius equal to unity in case (b) corresponds in case (c) to the rotating part of radius $1 + e_1$. Therefore we have

$$\frac{1 + e^{(c)}}{1 + e_1} = 1 + e^{(b)}, \tag{6.5}$$

where $e^{(b)}$ and $e^{(c)}$ denote the parameter e in cases (b) and (c). As in both cases time has been normalized by R^2 (where R is the dimensional radius of the rotor), in order to retrieve $\Omega^{(b)}$ from $\Omega^{(c)}$ we have to multiply (6.4) by $(1 + e_1)^2$. In addition, k_1 in case (c) is now equivalent to k in case (b). Furthermore, k' in cases (b) and (c) are equal (see Appendix E for a detailed proof). This implies that α in case (c) becomes α' in case (b), and that $C(\nu)$ and $F_{\sigma\mu}$ in case (b) are the same as those in case (c). This demonstrates that (6.4) and (5.2) are equivalent, and that case (c) with $e_1 \gg 1$ and $e = O(e_1)$ corresponds to case (b).

6.4. *Case (c) for $e = 0$*

Taking $e = 0$ implies that $e_1 = 0$, and then $k' = k_1 = k$, $k'_\sigma = k_\sigma$, $k'_\mu = k_\mu$ and $\alpha_1 = \beta_1 = \alpha' = \beta' = \alpha = \beta$. Then, $P(\nu) = -\varphi_\nu^{-1}(\Phi(k_\nu) + \Psi(k_\nu))(\Phi(k) + \Psi(k))$ and $Q(\nu) = -R(\nu) = \varphi_\nu^{-1}(\Phi(k) + \Psi(k))$, leading to

$$\Omega^{(c)}_{e=0} = -\frac{c}{s}\frac{(\Phi(k_\sigma) + \Psi(k_\sigma))(\Phi(k_\mu) + \Psi(k_\mu))}{\Phi(k_\sigma) + \Psi(k_\sigma) - \Phi(k_\mu) - \Psi(k_\mu)} \tag{6.6}$$

Applying the Wronskian (Abramowitz & Stegun 1968) given in (A 1) of Appendix A, leads to

$$\Omega^{(c)}_{e=0} = \frac{c}{s}(I_1(k_\sigma)K_1(k_\sigma) - I_1(k_\mu)K_1(k_\mu))^{-1}, \tag{6.7}$$

which is the dynamo threshold found in Plunian & Alboussière (2021).

6.5. *Case (c) for $e_1 = 0$*

Taking $e_1 = 0$ implies that $k_1 = k$, $\alpha_1 = \beta_1 = 1$, $\alpha = \alpha'$ and $\beta = \beta'$. Then $P(\nu) = \beta' A(\nu)D(\nu) - \alpha' B(\nu)C(\nu)$, $Q(\nu) = \alpha' C(\nu) - \beta' D(\nu)$, $R(\nu) = A(\nu) - B(\nu)$. Replacing in (5.3) leads to

$$\Omega^{(c)}_{e_1=0} = -\frac{c}{s}\frac{L(\sigma)L(\mu)}{E_{\sigma\mu}G(\sigma)G(\mu) + F_{\sigma\mu}H(\sigma)H(\mu)}, \tag{6.8}$$

with

$$L(\nu) = \beta' A(\nu)D(\nu) - \alpha' B(\nu)C(\nu), \tag{6.9a}$$

$$G(\nu) = \alpha' C(\nu) - \beta' D(\nu), \quad H(\nu) = A(\nu) - B(\nu). \tag{6.9b}$$

Now, the dispersion relation given in Plunian *et al.* (2025) can be rewritten as (see Appendix F).

$$\Omega_{2025} = \omega - \frac{c}{s}\frac{L(\sigma)L(\mu) + \frac{s}{c}\omega(1+e)^2\left(F_{\sigma\mu}M(\sigma)M(\mu) + \alpha'^2\beta'^2 E_{\sigma\mu}N(\sigma)N(\mu)\right)}{E_{\sigma\mu}G(\sigma)G(\mu) + F_{\sigma\mu}H(\sigma)H(\mu) + \frac{s}{c}\omega(1+e)^2(\alpha' - \beta')^2 F_{\sigma\mu}E_{\sigma\mu}}, \tag{6.10}$$

with

$$M(\nu) = -\alpha' B(\nu) + \beta' A(\nu), \quad N(\nu) = C(\nu) - D(\nu). \tag{6.11}$$

We note that $H(\nu)$ and $N(\nu)$ are related to each other by (A 5) given in Appendix A. This case corresponds to a rotating rotor at velocity Ω_{2025}, a stator at rest, both made of anisotropic material, and between both, a fluid layer rotating at velocity ω. Then, it is straightforward to show that (6.8) is equivalent to (6.10) for $\omega = 0$. Therefore, the case (c) for $e_1 = 0$ is equivalent to Plunian *et al.* (2025) with $\omega = 0$.

6.6. *Case (c) for $e_1 = e$*

For $e_1 = e$, we have $k_1 = k'$, $\alpha = \beta = 1$, $\alpha_1 = \alpha'$ and $\beta_1 = \beta'$. Then $P(\nu) = \frac{1}{\alpha'}A(\nu)D(\nu) - \frac{1}{\beta'}B(\nu)C(\nu)$, $Q(\nu) = C(\nu) - D(\nu)$, $R(\nu) = \frac{1}{\alpha'}A(\nu) - \frac{1}{\beta'}B(\nu)$. Replacing in (5.3), leads to

$$\Omega^{(c)}_{e_1=e} = -\frac{c}{s}\frac{1}{(1+e)^2}\frac{L(\sigma)L(\mu)}{F_{\sigma\mu}M(\sigma)M(\mu) + \alpha'^2\beta'^2 E_{\sigma\mu}N(\sigma)N(\mu)}. \tag{6.12}$$

Now taking $\omega = \Omega_{2025}$ in (6.10) leads to (6.12). Therefore, the case (c) for $e_1 = e$ is equivalent to Plunian *et al.* (2025) with $\omega = \Omega_{2025}$.

7. Results relevant to real-world applications

To quantify the effectiveness of the remote effect of electrical conductivity anisotropy or magnetic permeability anisotropy on the dynamo action, we consider four configurations (i) to (iv), relevant to real-world applications. The corresponding electromagnetic properties of the materials that will be considered are given in Table 1.

The dynamo threshold will be expressed in terms of the magnetic Reynolds number as given in $(3.15a-c)$, for two vertical magnetic modes defined as

$$k = n\pi R/H, \text{ with } n \in \{1, 2\}, \tag{7.1}$$

		Meta-material						Fluid				
Case	$T(^\circ\mathrm{C})$	$\sigma^\perp$	$\mu^\perp$	$\sigma^\parallel$	$\mu^\parallel$	σ	μ	Mat.	σ_F	μ_F	φ_σ	φ_μ
(i)	20	$\mathrm{Cu}^{(\perp)}$ 63	1	$\mathrm{Ka}^{(\parallel)}$ 5×10^{-22}	1	13×10^{22}	0	Ga	3.86	1	0.06	1
(iia) (iib)	100	$\mathrm{Cu}^{(\perp)}$ 47	1	$\mathrm{Ka}^{(\parallel)}$ 2.5×10^{-19}	1	19×10^{19}	0	Na	10.6	1	0.23	1
(iii)	100	$\mathrm{Fe}^{(\perp)}$ 6.9	5×10^{3}	$\mathrm{Na}^{(\parallel)}$ 10.6	1	-0.35	5×10^{3}	Na	10.6	1	1.53	2×10^{-4}
(iv)	4400	$\mathrm{Fe}^{(\perp)}$ 1	1	$\mathrm{Fe}^{(\parallel)}$ $(\sigma+1)^{-1}$	1	σ	0	$\mathrm{Fe}^{(\perp)}$	1	1	1	1

TABLE 1. Values of the electromagnetic properties taken for the four applications (i)-(iv). The electrical conductivities $\sigma^\perp$, $\sigma^\parallel$, $\sigma^\perp$ and $\sigma^\parallel$ are given in unit of $10^6\ \Omega^{-1}m^{-1}$. The magnetic permeabilities $\mu^\perp$, $\mu^\parallel$, $\mu^\perp$ and $\mu^\parallel$ are given in unit of $4\pi\times10^{-7}Hm^{-1}$. Their values have been taken from appropriate references (Jiles 1991; Gale & Totemeir 2004; Wu & Chung 2008; DuPont$^{\mathrm{TM}}$ 2006; Driscoll & Du 2019). The dimensionless parameters σ, μ, φ_σ and φ_μ are calculated from (2.7a-d).

where R and H are the radius and height of the rotor. They correspond to one period ($n=2$) or half a period ($n=1$) of the magnetic field across the height of the rotor. It is also interesting to express the dynamo threshold in terms of the rotor's frequency (in Hz), given by

$$f=\frac{|\Omega|}{2\pi R^2\sigma^\perp\mu^\perp}. \tag{7.2}$$

In all studied configurations, the pitch angle of the logarithmic anisotropy, for both the rotor and the stator, is set at $\alpha_q=0.15\pi$, simply because this is the one used in Fury's experiment, which, in this specific case, resulted in the minimum dynamo threshold. From now, e and e_1 denote dimensional quantities as depicted in figure 1.

The dynamo threshold will be plotted, and also the streamlines of the horizontal component of the magnetic field and the electric current, as well as the radial profile of their horizontal and vertical components. In addition to B_r, B_θ and J_z, whose expressions are given in equations (4.9)-(4.10)-(4.22) for case (a), (4.11)-(4.12)-(4.23) for case (b), and (4.13)-(4.14)-(4.24) for case (c), the derivation of the expressions of J_r, J_θ and B_z are given in Appendix G and H.

7.1. *Case (i)*

The first configuration corresponds to the design of an experiment currently under construction, called Furyfluid. Its geometry consists of a cylindrical layer of liquid galinstan, of thickness e, surrounded by a cylindrical rotor, on the inside, and by a cylindrical stator, on the outside, as the one depicted in figure 1c. The rotor and the stator are both made of an assembly of copper and kapton, making it the equivalent of a metamaterial with anisotropic electrical conductivity (see Table 1). In the experiment, four thicknesses of fluid layer will be investigated, $e/R\in\{0.029;0.257;0.486;0.714\}$. The dimensions of the rotor are R=7 cm in radius and H=30 cm in height, corresponding to $k=0.75$ (resp. $k=1.5$) for $n=1$ (resp. $n=2$).

In figure 2a, the marginal curves of the dynamo threshold are plotted versus e_1/R for the four values of e/R and two values of n. The left vertical scale corresponds to the rotor magnetic Reynolds number $Rm^{(i)}=|\Omega^{(c)}|$, with $\Omega^{(c)}$ given by (5.3), and the right vertical scale corresponds to the dimensional frequency $f^{(i)}$ given by (7.2). As e_1 varies from 0 to e, the value of e/R corresponding to each curve is given by the end of the curve, at $e_1/R=0.029$, 0.257, 0.486 or 0.714. The dynamo threshold for $n=1$ (black dashed curves) is found to be always smaller than the one for $n=2$ (blue solid curves), suggesting that in an experiment of finite size, the dominant magnetic mode at the threshold will be quadrupolar. Even for $e/R=0.01$, which corresponds to the thickness of the fluid layer of the experiment Fury, the dynamo threshold for $n=1$ is still the smallest, although the two dynamo thresholds are fairly close: $Rm^{(i)}$=16 (resp. 16.2) for $n=1$ (resp. $n=2$). This contrasts with the results of Fury in which an octupolar mode was generated (Alboussière *et al.* 2022). This discrepancy between the experimental and analytical results is most likely due to a finite-size effect that is only partially accounted for in this study.

From figure 2a it also appears that increasing the thickness e of the fluid gap leads to a larger dynamo threshold. To understand why, it is important to remember that the electrical conductivity anisotropy causes electric currents to be deflected in a way that is favourable to the dynamo effect. Having a fluid layer, whose electrical conductivity is isotropic, is therefore less efficient. It is the reason why, in Fury, the fluid layer has been minimised ($e/R=0.01$).

Finally, increasing e_1 from 0 to e implies that a greater volume of fluid will rotate, which should, mechanically speaking, lower the dynamo threshold. This is indeed the case, as $Rm^{(i)}(e_1=0)>Rm^{(i)}(e_1=e)$. However, the decrease of $Rm^{(i)}$ with e_1 is non-monotonic for $n=2$ and sufficiently large values of e. The dynamo threshold then reaches a maximum for an intermediate value of e_1/R. This is probably because the shear interacts mainly with the rotor at small values of e_1, and with the stator at large values of e_1. For intermediate values of e_1, as the shear effect is distant from both, the dynamo threshold can be higher. However, it is not clear why this does not hold for $n=1$.

In figures 2b and 2c, the streamlines of the magnetic field (resp. electric current density) are represented by blue solid (resp. red dashed) curves, for $e/R=0.714$, $e_1/R=0.3$, $n=1$ and $n=2$. In figures 2d and 2e, $B_H=\sqrt{B_r^2+B_\theta^2}$, $J_H=\sqrt{J_r^2+J_\theta^2}$, B_z and J_z are plotted versus r, with respectively blue solid, red dashed, black solid and black dashed lines. Within the rotor ($r\leqslant R$) and the stator ($r\geqslant R+e$), the electric current lines follow the helical structure imposed by the anisotropic electrical conductivity, and are radial within the fluid. We note that B_H is continuous, as expected from (3.9a,d,g) for B_r, from (3.9b,e,h) with $\mu=0$ and $\varphi_\mu=1$ for B_θ. In addition B_z is also continuous, as expected from (3.9c,f,i) for $\varphi_\mu=1$. From (3.13$a-c$), with $\varphi_\sigma\neq 1$ and $\Omega\neq 0$, J_z is expected to be discontinuous at $r=R, R+e_1, R+e$ as shown in figures 2c and 2d. Finally, J_H is discontinuous at $r=R, R+e$. To understand why, we can express J_r and J_θ as (G 1a,b), with $\tilde{\phi}$ defined in (4.18b). As $\varphi_\mu=1$ and $\mu=0$, J_r is continuous. However, it is the discontinuity of $\tilde{\sigma}$ given by (2.6b) that implies the discontinuity of J_θ at $r=R$ and $R+e$.

In figures 2d and 2e, we note that at $r=0$, $B_H=J_H=\partial B_z/\partial r=\partial J_z/\partial r=0$. This is also evident from the figures 4, 5d, 5e, 6d and 6e. The first boundary condition $B_H(r=0)=0$ corresponds to (3.1a,b). Then, (2.14a,b) and (3.1a,b) imply $D_k(B_r)=D_k(B_\theta)=0$ at $r=0$. Thus, with (2.16) and (3.6) we find that $\partial B_z/\partial r=0$ at $r=0$. Similarly, from (G 1a,b) and (4.18a,b) we find that $J_H=\partial J_z/\partial r=0$ at $r=0$.

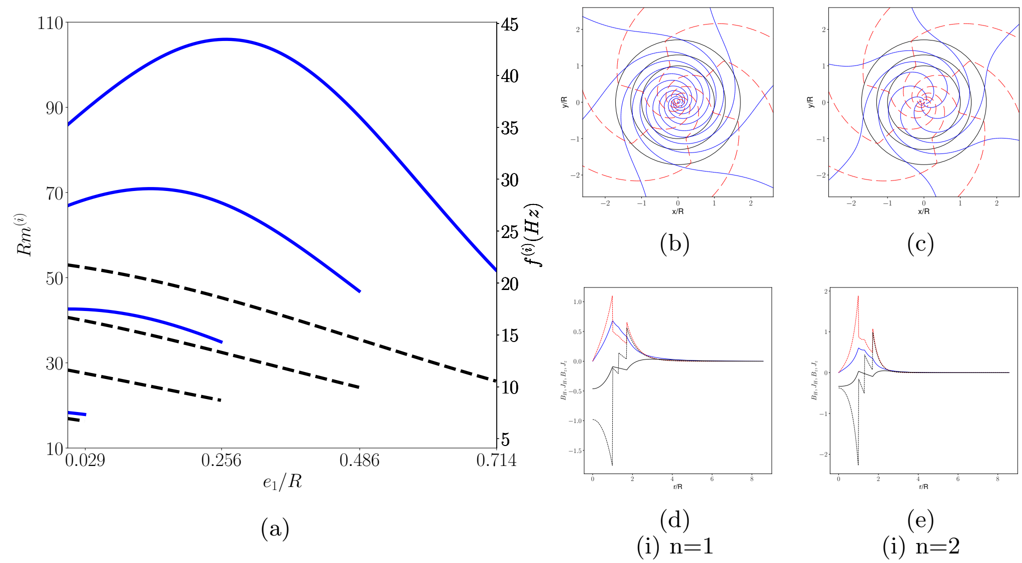

FIGURE 2. Case (i): A layer of galinstan is sandwiched between a rotor of radius R and a stator with an inner radius of $R+e$. The galinstan is sheared at a distance $e_1 \in [0, e]$ from the rotor. On the left (figure 2a), the dynamo threshold is plotted versus e_1 for four values of $e/R \in \{0.029; 0.257; 0.486; 0.714\}$ and two values of n. The black dashed (resp. solid blue) curves correspond to $n = 1$ (resp. $n = 2$). The vertical left (resp. right) axis corresponds to the rotor magnetic Reynolds number (resp. frequency in Hz). On the right (figures 2b-2e), the four figures correspond to $e/R = 0.714$ and $e_1/R = 0.3$, with $n = 1$ (b,d) or $n = 2$ (c,e). In figures 2b and 2c, the blue solid curves correspond to the magnetic streamlines, the red dashed curves to the electric current streamlines. In figures 2d and 2e, the blue solid, resp. red dashed, curve corresponds to $|B_H|$, resp. $|J_H|$, the black solid, resp. dashed, curve corresponds to B_z, resp. J_z.

7.2. *Cases (iia) and (iib)*

The second set of configurations is inspired by two other experiments, both conducted with liquid sodium, in Maryland (Adams *et al.* 2015) and Dresden (Stefani *et al.* 2024) respectively. The liquid sodium is contained in a large vessel, a spherical shell of 3 m in diameter in Maryland, a cylindrical vessel of 2 m by 2m in diameter and height in Dresden. In Maryland, differential rotation is produced by the rotation of a propeller (or an inner sphere) immersed in the centre of the vessel. In Dresden, the shear is produced by the precession of the cylindrical vessel. To assess the value of using an anisotropic material, i.e. a metamaterial made of an assembly of copper and kapton (see Table 1), we will study two cases, corresponding to (iia) immersing an anisotropic rotor (a rotor made of anisotropic material) in liquid sodium, or (iib) coating the wall of the vessel containing the liquid sodium with such anisotropic metamaterial. They correspond to the geometries (a) and (b) depicted in figure 1.

Case (iia)- Considering an anisotropic rotor with the same aspect ratio $H/R = 30/7$ as above, leads to the marginal curve $Rm^{(iia)} = |\Omega^{(a)}|$ versus e/R, which is plotted in figure 3a, for $n = 1$ (black dashed curve) and $n = 2$ (blue solid curve). For a rotor radius R=7 cm, the corresponding frequency (in Hz) is given on the right vertical axis. The dynamo threshold is minimized for $e = 0$, i.e. when the sodium is at rest. This means that the dynamo is the most efficient when the shear is at the edge of the rotor. We note a mode crossover at $e/R = 0.1$. For a finite size experiment, this suggests a change of mode from octupolar to quadrupolar as the shear moves away from the rotor edge.

Finally, if the shear is distant from the anisotropic wall, the dynamo still works, but the threshold increases with e. Of the two magnetic modes, by selecting the one that has the lowest dynamo threshold, the threshold for $e/R = 0$ is approximately doubled for $e/R = 0.5$.

Case (iib)- We consider an anisotropic stator of internal radius $R + e = R_{\max}$, a rotating motion of liquid sodium for $r \leqslant R$ and sodium at rest for $R \leqslant r \leqslant R_{\max}$. In addition, we assume that the height H of the stator is twice its radius, $H/R_{\max} = 2$. The dynamo threshold for the rotating part of sodium is plotted in figure 3b, as $Rm^{(iib)} = \varphi_\sigma \varphi_\mu |\Omega^{(b)}|$ versus $R/R_{\max} = (1 + e/R)^{-1}$. The vertical wave number defined by (7.1) varies linearly with $R/R_{\max}$ as $k = (n\pi/2)(R/R_{\max})$. The dynamo threshold is found to decrease with R, and is minimized at $R = R_{\max}$. This means that although the dynamo still works if the shear is distant from the anisotropic wall, it is minimum if the distance is zero. For $n = 1$ (resp. $n = 2$), the threshold for $R/R_{\max} = 1$ approximately doubles for $R/R_{\max} = 0.7$ (resp. 0.8). At $R = R_{\max}$, the frequency (in Hz) which is plotted in figure 3c, takes the value $f^{(iib)} = 0.16$ Hz for $n = 1$ ($k = 1.57$) and 0.22 Hz for $n = 2$ ($k = 3.14$) which are remarkably low values. Whilst the values of Rm in cases (iia) and (iib) are of the same order of magnitude, the frequency values differ by approximately two orders of magnitude. This is because the frequency is proportional to R^{-2} and inversely proportional to the electrical conductivity of the moving part, namely the rotor with radius $R = 7$ cm and conductivity $\sigma^\perp$ in case (iia), and the fluid of radius $R = 1$ m for $R = R_{\max}$ and conductivity σ_F in case (iib).

At top of figure 4, streamlines of the magnetic field (resp. electric current density) are represented by blue solid (resp. red dashed) curves, for (iia) $e/R = 0.5$, (iib) $e/R = 0.3$, and the two values $n = 1$ and $n = 2$. In case (iia), within the rotor ($r \leqslant R$) the electric currents follow the helical structure imposed by the anisotropic electrical conductivity, while they are oriented radially in the outer fluid ($r \geqslant R$). In case (iib), the electric currents are helical within the stator ($r \geqslant R + e$) where the electrical conductivity is anisotropic, and radial in the fluid ($r \leqslant R + e$). The magnetic field lines are also helical, with a significantly higher pitch angle in the fluid part. At bottom of figure 4, $B_H = \sqrt{B_r^2 + B_\theta^2}$, $J_H = \sqrt{J_r^2 + J_\theta^2}$, B_z and J_z are plotted versus r, with respectively blue solid, red dashed, black solid and black dashed lines. We note that B_H is continuous, as expected from (3.7a, b, d, e) in case (iia), from (3.8a, b, d, e) in case (iib), for $\mu = 0$ and $\varphi_\mu = 1$. Similarly, B_z is continuous, as expected from (3.7c) and (3.7f) in case (iia), from (3.8c) and (3.8f) in case (iib), for $\varphi_\mu = 1$. The discontinuity of J_H reflects the discontinuity of J_θ that occurs at the boundary between the anisotropic material and the fluid, at $r = R$ in case (iia), $r = R + e$ in case (iib). Finally, the discontinuity of J_z occurs at both $r = R$ and $r = R + e$, because of the discontinuity of φ_σ or Ω, as expected from (3.11a, b) in case (iia), (3.12a, b) in case (iib).

7.3. *Case (iii)*

As a third configuration, we revisit case (iia), but this time examining the remote effect of a magnetic permeability anisotropy rather than electrical conductivity, with reference to the VKS experiment (Monchaux *et al.* 2007). In the VKS experiment, the dynamo effect was obtained from a combination of shear maximum in the mid-plane of the experiment, and an α-effect taking place in the vicinity of the disks, thus separated by a certain distance, and with the α-effect being reinforced by the proximity of blades made of ferromagnetic material (soft iron) (Laguerre *et al.* 2008; Miralles *et al.* 2013). Although the geometry of VKS differs from that shown in figure 1a, it is interesting to quantify the effect of magnetic permeability anisotropy at a certain distance from shear

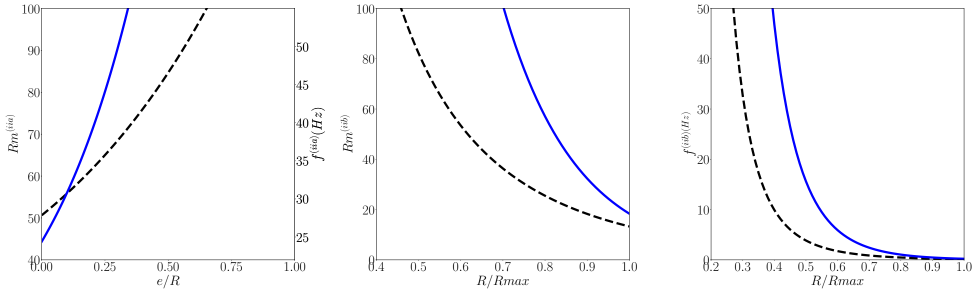

(a) (b) (c)

FIGURE 3. Figure 3a refers to case (iia): an anisotropic rotor of radius R immersed in liquid sodium, figures 3b and 3c to case (iib): an anisotropic stator of internal radius $R_{\max}$, containing liquid sodium. In figure 3a, the dynamo threshold is plotted versus e/R where e is the distance between the shear and the rotor. For $R = 7$ cm, the frequency (Hz) is indicated at the right axis. The black dashed (resp. solid blue) curve corresponds to a magnetic wave number $n = 1$ (resp. $n = 2$), i.e. a magnetic field of half a period (resp. one period) across the height of the rotor. In figure 3b, the dynamo threshold is plotted versus $R/R_{\max}$, where $R_{\max} - R$ is the distance between the shear and the stator. In figure 3c, the results are the same as in figure 3b, but expressed in terms of frequency. The black dashed (resp. solid blue) curve corresponds to $n = 1$ (resp. $n = 2$), i.e. a magnetic field of half a period (resp. one period) across the height of the stator.

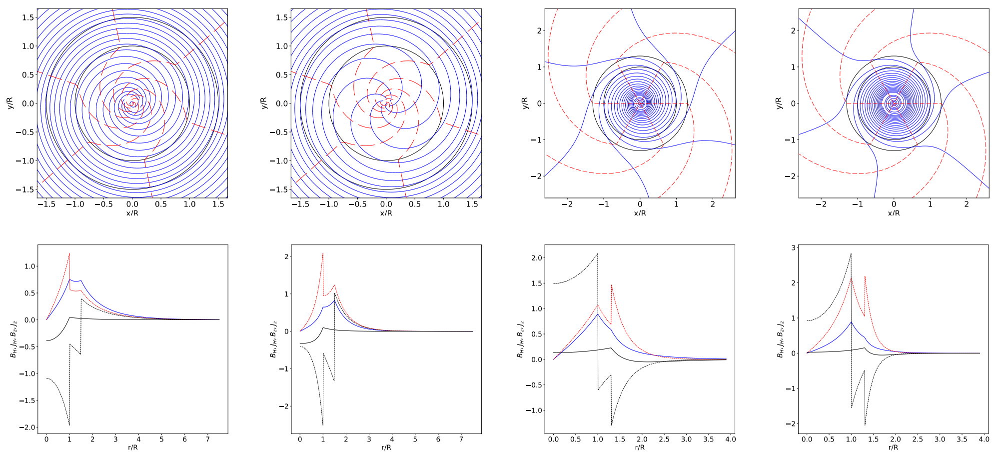

(iia) n=1 (iia) n=2 (iib) n=1 (iib) n=2

FIGURE 4. Streamlines and radial dependence in the cases (iia) for $e/R = 0.5$, (iib) for $e/R = 0.3$, and $n = 1$, or $n = 2$. On top, the blue solid curves correspond to the magnetic streamlines, the red dashed curves to the electric current streamlines. At bottom, the blue solid (resp. red dashed) curve corresponds to $|B_H|$ (resp. $|J_H|$). The black solid (resp. dashed) curve corresponds to B_z (resp. J_z).

in liquid sodium. To account for the effect of iron blades in liquid sodium, the rotor is taken as an assembly of two materials with the electromagnetic properties of iron and liquid sodium (see Table 1).

The marginal curves are plotted in figure 5a, for $n = 1$ (black dashed curve) and $n = 2$ (blue solid curve). The left (resp. right) vertical axis corresponds to the rotor frequency f in Hz (resp. $Rm^{(iii)} = |\Omega^{(a)}|$). The several orders of magnitude of $Rm^{(iii)}$ are due to the

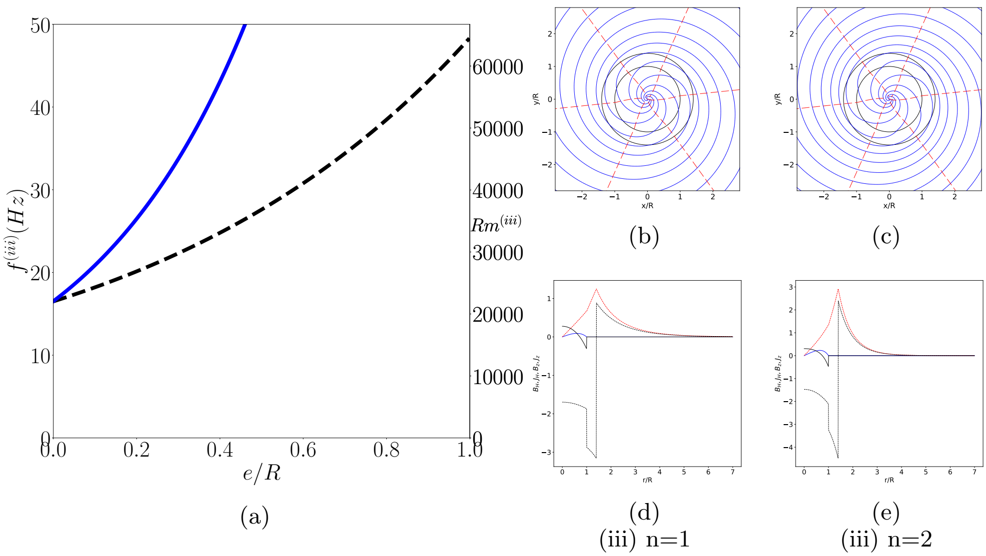

FIGURE 5. Case (iii)- A rotor of radius R, with an anisotropy of magnetic permeability, is immersed in liquid sodium. The sodium is sheared at a distance e from the rotor. On the left, in figure 5a, the dynamo threshold is plotted versus e/R for two values of n. The black dashed (resp. solid blue) curve corresponds to $n = 1$ (resp. $n = 2$). The vertical left (resp. right) axis corresponds to the rotor frequency in Hz (resp. magnetic Reynolds number). On the right, figures 5b-5e correspond to $e/R = 0.4$, with $n = 1$ (b,d) or $n = 2$ (c,e). In figures 5b and 5c, the blue solid curves correspond to the magnetic streamlines, the red dashed curves to the electric current streamlines. In figures 5d and 5e, the blue solid (resp. red dashed) curve corresponds to $|B_H|$, resp. $|J_H|$, the black solid (resp. dashed) curve corresponds to B_z, resp. J_z.

large values of $\mu^{\perp}$. Again, dynamo action works even though the shear is distant from the anisotropic rotor. The efficiency of the dynamo decreases with the distance between the shear and the anisotropic rotor, and the dynamo threshold for $n = 1$ (black dashed curve) is smaller than the one for $n = 2$ (blue solid curve). Finally, the threshold doubles for e/R increasing from 0 to 0.7 (resp. 0.3) for $n = 1$ (resp. $n = 2$).

In figures 5b and 5c, the streamlines of the magnetic field (resp. electric current density) are represented by blue solid (resp. red dashed) curves, for $e/R = 0.4$, and the two values $n = 1$ and $n = 2$. In figures 5d and 5e, $B_H = \sqrt{B_r^2 + B_\theta^2}$, $J_H = \sqrt{J_r^2 + J_\theta^2}$, B_z and J_z are plotted versus r, with respectively blue solid, red dashed, black solid and black dashed lines. Within the rotor ($r \leqslant R$) the magnetic field lines follow the helical structure imposed by the anisotropic magnetic permeability, and extend in the outer fluid ($r \geqslant R$) although with much less intensity by several orders of magnitude. The electric currents are almost radial in the rotor, and radial in the fluid.

We note that B_z is discontinuous at $r = R$, as expected from (3.7c) with $\varphi_\mu \neq 1$. As expected from (3.11a, b), J_z is also discontinuous, at both $r = R$ and $r = R + e$. In addition, and as expected from (3.7b) and (G 3), B_θ and J_θ are discontinuous at $r = R$, although this is not directly visible in figures 5d and 5e, without zooming in by several orders of magnitude. Finally, B_r and J_r are continuous at $r = R$ and $r = R + e$, as well as B_θ, J_θ and B_z at $r = R + e$. From figures 5d and 5e, we remark that the magnetic field is mainly concentrated in the rotor because of the high value of μ.

7.4. *Case (iv)*

In a fourth configuration, we revisit the geometry shown in figure 1(a), featuring an iron rotor immersed in molten iron, where the rotor exhibits a certain degree σ of electrical conductivity anisotropy. This refers to the Earth's core, assuming that the solid inner core has an anisotropic electrical conductivity and rotates with respect to the outer core. We have to consider a model of a cylindrical inner core instead of spherical. The shear might be localized in the tangent cylinder. In reality the distance between the inner core and the tangent cylinder depends on latitude, so that we take an unknown finite distance e in our cylindrical model.

We study how the dynamo threshold $Rm^{(iv)} = |\Omega^{(a)}|$ varies with σ, for $e/R \in \{0, 0.1, 0.3, 0.5, 1\}$ and $n \in \{1, 2\}$. In figure 6, the dynamo threshold is given in degree per year (left axis) for $R = 1220$ km, in addition to $Rm^{(iv)}$ (right axis). The results show that for σ of order unity or larger, and a rotation of a few tenths of a degree per year, the dynamo is indeed possible, provided the shear is not too distant. The magnetic mode n presenting the minimum dynamo threshold depends on e/R. It is $n = 2$ for $e/R \in \{0, 0.1\}$, $n = 1$ for $e/R \in \{0.5, 1\}$, with a mode crossover for $e/R = 0.3$.

In figures 6b and 6c, the streamlines of the magnetic field, resp. electric current density, are represented by blue solid (resp. red dashed) curves, for $e/R = 0.3$, and the two values $n = 1$ and $n = 2$. In figures 6d and 6e, $B_H = \sqrt{B_r^2 + B_\theta^2}$, $J_H = \sqrt{J_r^2 + J_\theta^2}$, B_z and J_z are plotted versus r, with respectively blue solid, red dashed, black solid and black dashed lines. Within the rotor ($r \leqslant R$) the electric current lines follow the helical structure imposed by the anisotropic electrical conductivity, and are radial in the outer fluid ($r \geqslant R$).

We note that B_H is continuous, as expected from $(3.7a, b, d, e)$. Similarly, B_z is continuous, as expected from $(3.7c, f)$. The discontinuity of J_H reflects that of J_θ occurring at the boundary between the anisotropic material and the fluid, at $r = R$. Finally, as $\varphi_\sigma = 1$, from $(3.11a)$ and $(3.7a)$, J_z is continuous at $r = R$. The discontinuity of J_z at $r = R + e$ comes from the discontinuity of Ω, as expected from $(3.11b)$.

8. Conclusions

We have demonstrated that a dynamo effect can be generated by simple shear in an electrically conducting fluid, provided that a wall made of a material with anisotropic electrical conductivity or anisotropic magnetic permeability is placed not too far away. Three configurations were considered: when the anisotropic material is immersed in the fluid, when the fluid is contained within the anisotropic material, and when the fluid is sandwiched between two anisotropic materials. In the first two configurations, the dynamo threshold increases with the distance between the shear in the fluid and the wall. In the third one, the results depend on the distance between the two walls, and the dynamo threshold may therefore exhibit non-monotonic behaviour as a function of the shear position. According to the aspect ratio of the geometry, the magnetic vertical mode which is generated may also vary with the distance between the shear layer and the wall.

In order to assess the suitability of an anisotropic dynamo for practical applications, and given that the results depend on the electromagnetic properties of the wall and the fluid, we examined four configurations inspired either by dynamo experiments (i–iii) or by the Earth's core (iv). Even though the actual geometries differ from those of our models (e.g. cylindrical rather than spherical), the results indicate dynamo threshold values that are either experimentally achievable (cases (i-iii)), or consistent with observations (case

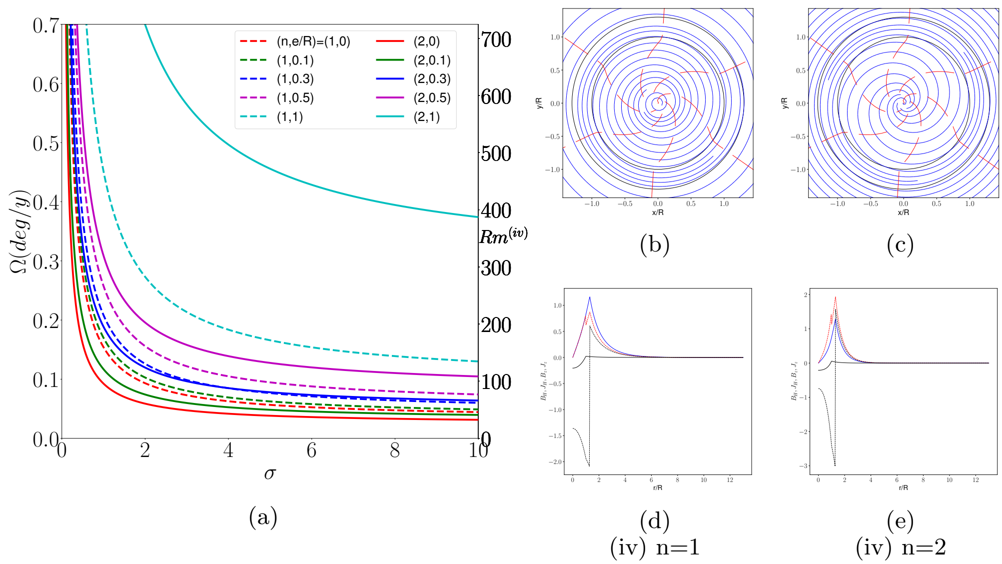

FIGURE 6. Case (iv)- On the right, in figure 6a, the dynamo threshold Ω is plotted versus the degree of anisotropy σ of an iron rotor of radius $R = 1220$ km, immersed in liquid iron. The value of Ω is given in degrees per year (resp. $Rm^{(iv)}$) on the left-hand axis (resp. right-hand axis). The colors correspond to different values of e/R. The dashed (resp. solid) curves correspond to $n = 1$ (resp. $n = 2$). The colors (resp. red, green, blue, magenta and cyan) correspond to different values of e/R (resp. $e/R = 0, 0.1, 0.3, 0.5, 1$). On the right, the four figures 6b-6e correspond to $e/R = 0.3$, with $n = 1$ (b,d) or $n = 2$ (c,e). In figures 6b and 6c, the blue solid curves correspond to the magnetic streamlines, the red dashed curves to the electric current streamlines. In figures 6d and 6e, the blue solid (resp. red dashed) curve corresponds to $|B_H|$ (resp. $|J_H|$) the black solid (resp. dashed) curve corresponds to B_z (resp. J_z).

(iv)), provided, however, that the distance between the shear layer and the wall does not exceed approximately half the radius of the rotor or stator.

In case (i), a galinstan layer is sandwiched between a rotor and a stator, both made of an assembly of copper and kapton (the anisotropic metamaterial used in Fury). The results support the idea of using a layer of galinstan thicker than in Fury, which is in line with the design of a future dynamo experiment.

In case (iia), a rotor made from the same metamaterial as in Fury is immersed in liquid sodium, inspired by the spherical Couette experiment conducted in Maryland. In case (iib), a container – also made of the same metamaterial – contains liquid sodium, inspired by the Dresdyn precession experiment. In both cases, the results indicate a low dynamo threshold, which opens up new possibilities through the incorporation of an anisotropic wall.

In case (iii), a rotor made of an assembly of soft iron and sodium is immersed in liquid sodium. The results confirm the role of high magnetic permeability, as had already been demonstrated by the VKS experiment (Miralles *et al.* 2013).

In case (iv), a rotor made of an anisotropic crystal of iron is immersed in liquid iron. At the scale of a planet like Earth, the results of case (iv) suggest that a dynamo could be driven by a large-scale shear flow within the outer core, provided that some appropriate anisotropy of electrical conductivity exists in the inner core.

The inner core is known to exhibit seismic anisotropy of P waves of a few percents in celerity (Deuss 2014; Ohta *et al.* 2018; Das *et al.* 2026), and could be associated with some anisotropy of electrical conductivity. Rotation of the inner core is believed to exist (Song & Richards 1996; Tkalčić *et al.* 2013) under the form of alternative oscillations for tens of years eastward or westward around an averaged gravitational locked position with respect to the mantle (Alboussière *et al.* 2010). Inner core rotation is not even required for the application of our model: shear due to any zonal flow in the outer core would be equally suitable.

Acknowledgements

The authors thank R. Claveau for a careful reading that led to a significant improvement of the paper.

REFERENCES

Abramowitz, M. & Stegun, I. A. 1968 *Handbook of Mathematical Functions with Formulas, Graphs and Mathematical Tables*. Dover Publications, New York.

Adams, M.M., Stone, D.R., Zimmerman, D.S. & Lathrop, D.P. 2015 Liquid sodium models of the Earth's core. *Prog. Earth Planet. Sci.* **29**, 1–18.

Alboussière, T., Drif, K. & Plunian, F. 2020 Dynamo action in sliding plates of anisotropic electrical conductivity. *Phys. Rev. E* **101**, 033107.

Alboussière, T., Plunian, F. & Moulin, M. 2022 Fury: an experimental dynamo with anisotropic electrical conductivity. *Proc. R. Soc. A* **478**, 20220374.

Alboussière, T., Deguen, R. & Melzani, M. 2010 Melting-induced stratification above the Earth's inner core due to convective translation. *Nature* **466**, 744–747.

Avalos-Zúñiga, R. & Priede, J. 2023 Realization of bullard's disc dynamo. *Proc. R. Soc. A* **479**, 20220740.

Bullard, E. 1955 The stability of a homopolar dynamo. *Math. Proc. Camb. Philos. Soc.* **51** (4), 744–760.

Childress, S. & Gilbert, A. D. 1995 *Stretch, Twist, Fold: The Fast Dynamo*. Springer.

Cowling, T. G. 1934 The magnetic field of sunspots. *Mon. Not. R. Astr. Soc.* **94**, 39–48.

Das, P.P., Buffett, B. & Frost, D. 2026 Generation of inner core anisotropy by anisotropic thermal conductivity of iron crystals. *Nat. Geosci.* **19**, 353–358.

Deuss, A. 2014 Heterogeneity and anisotropy of Earth's inner core. *Annu. Rev. Earth and Planet. Sci.* **42** (1), 103–126.

Driscoll, P. E. & Du, Z. 2019 Geodynamo conductivity limits. *Geophys. Res. Lett.* **46**, 7982–7989.

DuPont™ 2006 *Summary of Properties*. Online at https://docs.rs-online.com/c6e2/0900766b80659d8c.pdf (accessed June 2026).

Favier, B. & Proctor, M. R. E. 2013 Growth rate degeneracies in kinematic dynamos. *Phys. Rev. E* **88**, 031001.

Gale, W.F. & Totemeir, T.C. 2004 *Smithells Metal Reference Book*.

Gilbert, A. D. 1988 Fast dynamo action in the Ponomarenko dynamo. *Geophys. Astrophys. Fluid Dyn.* **44** (1-4), 241–258.

Gilbert, A. D. 2003 Chapter 9 - Dynamo Theory. *Handbook of Mathematical Fluid Dynamics*, vol. 2, pp. 355–441. North-Holland.

Gomez, P., Plunian, F. & Alboussière, T. 2025 Can the dynamo of spiral-arm galaxies be explained by anisotropic conductivity? *Astrophys. J.* **981** (2), 164.

Herzenberg, A. 1958 Geomagnetic dynamos. *Philos. Trans. R. Soc. Lond. A* **250** (986), 543–583.

Jiles, D. 1991 *Introduction to Magnetism and Magnetic materials*. Springer.

Jones, C.A., Thompson, M.J. & Tobias, S.M. 2010 The solar dynamo. *Space Sci. Rev.* **152**, 591–616.

Krause, F. & Rädler, K. H. 1980 *Mean-field magnetohydrodynamics and dynamo theory*. Oxford: Pergamon Press, 1980.

Laguerre, R., Nore, C., Ribeiro, A., Léorat, J., Guermond, J.-L. & Plunian, F. 2008

Impact of impellers on the axisymmetric magnetic mode in the VKS dynamo experiment. *Phys. Rev. Lett.* **101**, 104501.

Marcotte, F., Gallet, B., Pétrélis, F. & Gissinger, C. 2021 Enhanced dynamo growth in nonhomogeneous conducting fluids. *Phys. Rev. E* **104**, 015110.

Miralles, S., Bonnefoy, N., Bourgoin, M., Odier, P., Pinton, J.-F., Plihon, N., Verhille, G., Boisson, J., Daviaud, F. & Dubrulle, B. 2013 Dynamo threshold detection in the von Kármán sodium experiment. *Phys. Rev. E* **88**, 013002.

Moffatt, H. K. 1978 *Magnetic Field Generation in Electrically Conducting Fluids*. Cambridge University Press, Cambridge, England.

Monchaux, R., Berhanu, M., Bourgoin, M., Moulin, M., Odier, Ph., Pinton, J.-F., Volk, R., Fauve, S., Mordant, N., Pétrélis, F., Chiffaudel, A., Daviaud, F., Dubrulle, B., Gasquet, C., Marié, L. & Ravelet, F. 2007 Generation of a magnetic field by dynamo action in a turbulent flow of liquid sodium. *Phys. Rev. Lett.* **98**, 044502.

Ohta, K., Nishihara, Y., Sato, Y., Hirose, K., Yagi, T., Kawaguchi, S. I., Hirao, N. & Ohishi, Y. 2018 An experimental examination of thermal conductivity anisotropy in hcp iron. *Front. Earth Sci.* **6**, 176.

Plunian, F. & Alboussière, T. 2020 Axisymmetric dynamo action is possible with anisotropic conductivity. *Phys. Rev. Res.* **2**, 013321.

Plunian, F. & Alboussière, T. 2021 Axisymmetric dynamo action produced by differential rotation, with anisotropic electrical conductivity and anisotropic magnetic permeability. *J. Plasma Phys.* **87** (1), 905870110.

Plunian, F. & Alboussière, T. 2022 Fast and furious dynamo action in the anisotropic dynamo. *J. Fluid Mech.* **87**, A66.

Plunian, F. & Alboussière, T. 2023 Dynamo action produced by an anisotropic rotor immersed in an electrically conducting medium at rest. *Phys. Rev. Fluids* **8**, 113702.

Plunian, F., Gomez, P. & Alboussière, T. 2025 Three-body anisotropic dynamo: the rotor, the gap and the stator. *C. R. Phys.* **26**, 295–315.

Priede, J. & Avalos-Zúñiga, R. 2013 Feasible homopolar dynamo with sliding liquid-metal contacts. *Physics Letters A* **377** (34), 2093 – 2096.

Ruderman, M. S. & Ruzmaikin, A. A. 1984 Magnetic field generation in an anisotropically conducting fluid. *Geophys. Astrophys. Fluid Dyn.* **28** (1), 77–88.

Ruzmaikin, A., Sokoloff, D. & Shukurov, A. 1988 Hydromagnetic screw dynamo. *J. Fluid Mech.* **197**, 39–56.

Rädler, K-H & Rheinhardt, M. 2002 Can a disc dynamo work in the laboratory? *Magnetohydrodynamics* **38**, 211–217.

Song, X. & Richards, P. 1996 Seismological evidence for differential rotation of the Earth's inner core. *Nature* **382**, 221–224.

Soward, A. M. 1987 Fast dynamo action in a steady flow. *J. Fluid Mech.* **180**, 267–295.

Steenbeck, M., Krause, F. & Rädler, K.-H. 1966 A calculation of the mean electromotive force in an electrically conducting fluid in turbulent motion, under the influence of coriolis forces. *Zeitschrift für Naturforschung* **21A**, 369–376, [English transl.: Roberts, P.H. & Stix, M., Tech. Note NCRA Boulder Colorado, 60, 29-47 (1971)].

Stefani, F., Anders, S., Eckert, S., Freyer, N., Gerbeth, G., Giesecke, A., Gundrum, T., Kaever, P., Kumar, V., Pizzi, F., Räbiger, D., Šimkanin, J., Steglich, C., Vogt, T., Wagner, N. & Wedel, G. 2024 The dresdyn precession experiment. *C. R. Phys.* **25** (S3), 629–647.

Tkalčić, H., Young, M., Bodin, T., Ngo, S. & Sambridge, M. 2013 The shuffling rotation of the Earth's inner core revealed by earthquake doublets. *Nature Geoscience* **6**, 497–502.

Tobias, S.M. 2021 The turbulent dynamo. *J. Fluid Mech.* **912**, P1.

Vainshtein, S.I. & Zel'dovich, Ya. B. 1972 Origin of magnetic fields in astrophysics. *Usp. Fiz. Nauk* **106**, 431–457, [English transl.: Sov. Phys. Usp., Vol. 15, p. 159-172, 1972].

Weiss, N.O. & Thompson, N.O. 2009 The solar dynamo. *Space Sci. Rev.* **144**, 53–66.

Wu, J. & Chung, D.D.L. 2008 Combined use of magnetic and electrically conductive fillers in a polymer matrix for electromagnetic interference shielding. *J. Electron. Mater.* **37**, 1088–1094.

Appendix A. Useful relations

The Wronskian (Abramowitz & Stegun 1968)

$$x\frac{I_0(x)}{I_1(x)} + x\frac{K_0(x)}{K_1(x)} = (I_1(x)K_1(x))^{-1}, \tag{A 1}$$

implies

$$\Phi(k) + \Psi(k) = \alpha_1\beta_1\left(\Phi(k_1) + \Psi(k_1)\right), \tag{A 2a}$$
$$\Phi(k_1) + \Psi(k_1) = \alpha\beta\left(\Phi(k') + \Psi(k')\right), \tag{A 2b}$$
$$\Phi(k) + \Psi(k) = \alpha'\beta'\left(\Phi(k') + \Psi(k')\right). \tag{A 2c}$$

From (5.4d, e), we have

$$\Phi(k) + \Psi(k) = -\varphi_\nu\left(A(\nu) - B(\nu)\right), \tag{A 3a}$$
$$\Phi(k') + \Psi(k') = \varphi_\nu\left(C(\nu) - D(\nu)\right). \tag{A 3b}$$

Then, (A 2c) and (A 3a, b) imply

$$B(\nu) - A(\nu) = \alpha'\beta'(C(\nu) - D(\nu)), \tag{A 4}$$

where $A(\nu), B(\nu), C(\nu), D(\nu)$ are defined in (5.4c, d), or equivalently

$$H(\nu) = -\alpha'\beta' N(\nu), \tag{A 5}$$

where $H(\nu)$ and $N(\nu)$ are defined in (6.9b) and (6.11). Then we have

$$\Phi(k) + \Psi(k) = -\varphi_\nu H(\nu), \tag{A 6a}$$
$$\Phi(k') + \Psi(k') = -\varphi_\nu(\alpha'\beta')^{-1}H(\nu), \tag{A 6b}$$

leading to

$$\left(\Phi(k) + \Psi(k)\right)\left(\Phi(k') + \Psi(k')\right) = \varphi_\sigma\varphi_\mu(\alpha'\beta')^{-1}H(\sigma)H(\mu), \tag{A 7}$$

or, equivalently, to

$$\left(\Phi(k) + \Psi(k)\right)\left(\Phi(k') + \Psi(k')\right) = \varphi_\sigma\varphi_\mu\alpha'\beta' N(\sigma)N(\mu). \tag{A 8}$$

Appendix B. Derivation of the dynamo threshold (5.1) for case (a)

The system (4.15$a - f$), (4.25a, b) can be written as

$$\lambda_r^I + \lambda_r^K = \lambda_\sigma^R + \lambda_\mu^R, \tag{B 1a}$$
$$\varphi_\mu^{-1}\left(\lambda_\theta^I + \lambda_\theta^K\right) = \lambda_\sigma^R, \tag{B 1b}$$
$$-\varphi_\mu^{-1}\left(-\lambda_r^I\Phi(k) + \lambda_r^K\Psi(k)\right) = \lambda_\sigma^R\Phi(k_\sigma) + \lambda_\mu^R\Phi(k_\mu), \tag{B 1c}$$
$$\lambda_r^I\alpha' + \lambda_r^K\beta' = \lambda_r^S, \tag{B 1d}$$
$$\lambda_\theta^I\alpha' + \lambda_\theta^K\beta' = \lambda_\theta^S, \tag{B 1e}$$
$$-\lambda_r^I\alpha'\Phi(k') + \lambda_r^K\beta'\Psi(k') = \lambda_r^S\Psi(k'), \tag{B 1f}$$
$$\varphi_\sigma^{-1}\varphi_\mu^{-1}\left(\lambda_\theta^I\Phi(k) - \lambda_\theta^K\Psi(k)\right) = \lambda_\sigma^R\Phi(k_\sigma), \tag{B 1g}$$
$$\lambda_\theta^I\alpha'\Phi(k') - \lambda_\theta^K\beta'\Psi(k') - \Omega^*\left(\lambda_r^I\alpha' + \lambda_r^K\beta'\right) = -\lambda_\theta^S\Psi(k'), \tag{B 1h}$$

with

$$(k', k'_\sigma, k'_\mu) = (1+e)(k, k_\sigma, k_\mu), \quad k_\sigma = k\left(\tfrac{1+\sigma}{1+\sigma s^2}\right)^{1/2}, \quad k_\mu = k\left(\tfrac{1+\mu}{1+\mu s^2}\right)^{1/2}, \tag{B 2a}$$

$$\Omega^* = \varphi_\sigma\varphi_\mu\Omega\tfrac{s}{c}(1+e)^2, \Phi(x) = x\tfrac{I_0(x)}{I_1(x)}, \Psi(x) = x\tfrac{K_0(x)}{K_1(x)}, \alpha' = \tfrac{I_1(k')}{I_1(k)}, \beta' = \tfrac{K_1(k')}{K_1(k)}. \tag{B 2b}$$

The system (B 1$a-h$) is thus represented by the following 8 × 8 matrix

$$\begin{bmatrix} -1 & -1 & 1 & 1 & 0 & 0 & 0 & 0 \\ -1 & 0 & 0 & 0 & \varphi_\mu^{-1} & \varphi_\mu^{-1} & 0 & 0 \\ -\Phi(k_\sigma) & -\Phi(k_\mu) & \varphi_\mu^{-1}\Phi(k) & -\varphi_\mu^{-1}\Psi(k) & 0 & 0 & 0 & 0 \\ 0 & 0 & \alpha' & \beta' & 0 & 0 & -1 & 0 \\ 0 & 0 & 0 & 0 & \alpha' & \beta' & 0 & -1 \\ 0 & 0 & -\alpha'\Phi(k') & \beta'\Psi(k') & 0 & 0 & -\Psi(k') & 0 \\ -\varphi_\sigma\varphi_\mu\Phi(k_\sigma) & 0 & 0 & 0 & \Phi(k) & -\Psi(k) & 0 & 0 \\ 0 & 0 & -\alpha'\Omega^* & -\beta'\Omega^* & \alpha'\Phi(k') & -\beta'\Psi(k') & 0 & \Psi(k') \end{bmatrix}. \tag{B 3}$$

As (B 1$a-h$) must be singular, the determinant of this matrix must be set to zero. Then, by making linear combinations of lines or columns (where c_n and l_m mean column n and line m respectively), we will simplify this determinant in a succession of steps, at each step the determinant being equal to zero. First let us subtract $\Phi(k_\mu)l_1$ to l_3, subtract $\Psi(k')l_4$ to l_6, and add $\Psi(k')l_5$ to l_8. This leads to the following 4 × 4 determinant

$$\begin{vmatrix} -1 & 0 & \varphi_\mu^{-1} & \varphi_\mu^{-1} \\ -E_{\sigma\mu} & -B(\mu) & 0 & 0 \\ -\varphi_\sigma\varphi_\mu\Phi(k_\sigma) & 0 & \Phi(k) & -\Psi(k) \\ 0 & -\beta'\Omega^* & \alpha'[\Phi(k')+\Psi(k')] & 0 \end{vmatrix} = 0, \tag{B 4}$$

where $E_{\sigma\mu} = \Phi(k_\sigma) - \Phi(k_\mu)$ and $B(\nu) = \Phi(k_\nu) + \varphi_\nu^{-1}\Psi(k)$. Then, adding $\varphi_\mu^{-1}c_1$ to c_3 and c_4, leads to the 3 × 3 determinant

$$\begin{vmatrix} -B(\mu) & -\varphi_\mu^{-1}E_{\sigma\mu} & -\varphi_\mu^{-1}E_{\sigma\mu} \\ 0 & -\varphi_\sigma A(\sigma) & -\varphi_\sigma B(\sigma) \\ -\beta'\Omega^* & \alpha'[\Phi(k')+\Psi(k')] & 0 \end{vmatrix} = 0, \tag{B 5}$$

where $A(\nu) = \Phi(k_\nu) - \varphi_\nu^{-1}\Phi(k)$. After developing this determinant, and noticing that $B(\nu) - A(\nu) = \varphi_\nu^{-1}[\Phi(k)+\Psi(k)]$, the following expression can be derived

$$\alpha' B(\sigma)B(\mu)[\Phi(k')+\Psi(k')] + \beta'\varphi_\sigma^{-1}\varphi_\mu^{-1}E_{\sigma\mu}[\Phi(k)+\Psi(k)]\Omega^* = 0. \tag{B 6}$$

Then, using the relation (A 2c) leads to (5.1).

Appendix C. Derivation of the dynamo threshold (5.2) for case (b)

The system (4.16$a-f$), (4.26a,b) can be written as

$$\lambda_r^I + \lambda_r^K = \lambda_r^R, \tag{C 1a}$$

$$\lambda_\theta^I + \lambda_\theta^K = \lambda_\theta^R, \tag{C 1b}$$

$$\lambda_r^I\Phi(k) - \lambda_r^K\Psi(k) = \lambda_r^R\Phi(k), \tag{C 1c}$$

$$\lambda_r^I\alpha' + \lambda_r^K\beta' = \lambda_\sigma^S + \lambda_\mu^S, \tag{C 1d}$$

$$\varphi_\mu^{-1}\lambda_\theta^I\alpha' + \varphi_\mu^{-1}\lambda_\theta^K\beta' = \lambda_\sigma^S, \tag{C 1e}$$

$$-\varphi_\mu^{-1}\lambda_r^I\alpha'\Phi(k') + \varphi_\mu^{-1}\lambda_r^K\beta'\Psi(k') = \lambda_\sigma^S\Psi(k'_\sigma) + \lambda_\mu^S\Psi(k'_\mu), \tag{C 1f}$$

$$\lambda_\theta^I\Phi(k) - \lambda_\theta^K\Psi(k) = \lambda_\theta^R\Phi(k) - \Omega^*\lambda_r^R, \tag{C 1g}$$

$$\lambda_\theta^I\alpha'\Phi(k') - \lambda_\theta^K\beta'\Psi(k') = -\varphi_\sigma\varphi_\mu\lambda_\sigma^S\Psi(k'_\sigma), \tag{C 1h}$$

with

$$(k', k'_\sigma, k'_\mu) = (1+e)(k, k_\sigma, k_\mu), \quad k_\sigma = k\left(\frac{1+\sigma}{1+\sigma s^2}\right)^{1/2}, \quad k_\mu = k\left(\frac{1+\mu}{1+\mu s^2}\right)^{1/2}, \quad (\mathrm{C}\,2a)$$

$$\Omega^* = \varphi_\sigma\varphi_\mu\Omega\frac{s}{c}, \Phi(x) = x\frac{I_0(x)}{I_1(x)}, \Psi(x) = x\frac{K_0(x)}{K_1(x)}, \alpha' = \frac{I_1(k')}{I_1(k)}, \beta' = \frac{K_1(k')}{K_1(k)}. \quad (\mathrm{C}\,2b)$$

The system (C 1$a-h$) is thus represented by an 8×8 matrix with the following order for the variables $\lambda_r^R, \lambda_\theta^R, \lambda_r^I, \lambda_r^K, \lambda_\theta^I, \lambda_\theta^K, \lambda_\sigma^S, \lambda_\mu^S$,

$$\begin{bmatrix} -1 & 0 & 1 & 1 & 0 & 0 & 0 & 0 \\ 0 & -1 & 0 & 0 & 1 & 1 & 0 & 0 \\ -\Phi(k) & 0 & \Phi(k) & -\Psi(k) & 0 & 0 & 0 & 0 \\ 0 & 0 & \alpha' & \beta' & 0 & 0 & -1 & -1 \\ 0 & 0 & 0 & 0 & \varphi_\mu^{-1}\alpha' & \varphi_\mu^{-1}\beta' & -1 & 0 \\ 0 & 0 & -\varphi_\mu^{-1}\alpha'\Phi(k') & \varphi_\mu^{-1}\beta'\Psi(k') & 0 & 0 & -\Psi(k'_\sigma) & -\Psi(k'_\mu) \\ \Omega^* & -\Phi(k) & 0 & 0 & \Phi(k) & -\Psi(k) & 0 & 0 \\ 0 & 0 & 0 & 0 & \alpha'\Phi(k') & -\beta'\Psi(k') & \varphi_\sigma\varphi_\mu\Psi(k'_\sigma) & 0 \end{bmatrix}. \quad (\mathrm{C}\,3)$$

As (C 1$a-h$) must be singular, the determinant of this matrix must be set to zero. Then, by making linear combinations of lines or columns (where c_n and l_m mean column n and line m respectively), we will simplify this determinant in a succession of steps, at each step the determinant being equal to zero. First let us add c_1 to c_3 and c_4, add c_2 to c_5 and c_6. This leads to the following 5×5 determinant

$$\begin{vmatrix} \alpha' & 0 & 0 & -1 & -1 \\ 0 & \varphi_\mu^{-1}\alpha' & \varphi_\mu^{-1}\beta' & -1 & 0 \\ -\varphi_\mu^{-1}\alpha'\Phi(k') & 0 & 0 & -\Psi(k'_\sigma) & -\Psi(k'_\mu) \\ \Omega^* & 0 & -[\Phi(k)+\Psi(k)] & 0 & 0 \\ 0 & \alpha'\Phi(k') & -\beta'\Psi(k') & \varphi_\sigma\varphi_\mu\Psi(k'_\sigma) & 0 \end{vmatrix} = 0. \quad (\mathrm{C}\,4)$$

Then, dividing c_2 by α', adding $\alpha' c_5$ to c_1, subtracting c_5 to c_4, dividing c_3 by β' and multiplying l_4 by β' leads to the following 4×4 determinant

$$\begin{vmatrix} 0 & \varphi_\mu^{-1} & \varphi_\mu^{-1} & -1 \\ -\alpha' C(\mu) & 0 & 0 & -F_{\sigma\mu} \\ \Omega^*\beta' & 0 & -[\Phi(k)+\Psi(k)] & 0 \\ 0 & \Phi(k') & -\Psi(k') & \varphi_\sigma\varphi_\mu\Psi(k'_\sigma) \end{vmatrix} = 0, \quad (\mathrm{C}\,5)$$

where $C(\nu) = \Psi(k'_\nu) + \varphi_\nu^{-1}\Phi(k')$ and $F_{\sigma\mu} = \Psi(k'_\sigma) - \Psi(k'_\mu)$. Adding $\varphi_\mu^{-1} c_4$ to c_2 and c_3 leads to the following 3×3 determinant

$$\begin{vmatrix} -\alpha' C(\mu) & -\varphi_\mu^{-1}F_{\sigma\mu} & -\varphi_\mu^{-1}F_{\sigma\mu} \\ \Omega^*\beta' & 0 & -[\Phi(k)+\Psi(k)] \\ 0 & \varphi_\sigma C(\sigma) & \varphi_\sigma D(\sigma) \end{vmatrix} = 0, \quad (\mathrm{C}\,6)$$

where $D(\nu) = \Psi(k'_\nu) - \varphi_\nu^{-1}\Psi(k')$. After developing this determinant, the following expression can be derived

$$\alpha' C(\sigma)C(\mu)[\Phi(k)+\Psi(k)] - \beta'\varphi_\mu^{-1}F_{\sigma\mu}[D(\sigma) - C(\sigma)]\Omega^* = 0. \quad (\mathrm{C}\,7)$$

Then, using (A 2c) and (A 3b) leads to (5.2).

Appendix D. Derivation of the dynamo threshold (5.3) for case (c)

The system $(4.17a-i)$, $(4.27a-c)$ can be written as

$$\lambda^I_{r_1}+\lambda^K_{r_1}=\lambda^R_\sigma+\lambda^R_\mu, \tag{D 1a}$$
$$\varphi_\mu^{-1}\left(\lambda^I_{\theta_1}+\lambda^K_{\theta_1}\right)=\lambda^R_\sigma, \tag{D 1b}$$
$$-\varphi_\mu^{-1}\left(-\lambda^I_{r_1}\Phi(k)+\lambda^K_{r_1}\Psi(k)\right)=\lambda^R_\sigma\Phi(k_\sigma)+\lambda^R_\mu\Phi(k_\mu), \tag{D 1c}$$
$$\lambda^I_{r_1}\alpha_1+\lambda^K_{r_1}\beta_1=\lambda^I_{r_2}+\lambda^K_{r_2}, \tag{D 1d}$$
$$\lambda^I_{\theta_1}\alpha_1+\lambda^K_{\theta_1}\beta_1=\lambda^I_{\theta_2}+\lambda^K_{\theta_2}, \tag{D 1e}$$
$$-\lambda^I_{r_1}\alpha_1\Phi(k_1)+\lambda^K_{r_1}\beta_1\Psi(k_1)=-\lambda^I_{r_2}\Phi(k_1)+\lambda^K_{r_2}\Psi(k_1), \tag{D 1f}$$
$$\lambda^I_{r_2}\alpha+\lambda^K_{r_2}\beta=\lambda^S_\sigma+\lambda^S_\mu, \tag{D 1g}$$
$$\varphi_\mu^{-1}\left(\lambda^I_{\theta_2}\alpha+\lambda^K_{\theta_2}\beta\right)=\lambda^S_\sigma, \tag{D 1h}$$
$$\varphi_\mu^{-1}\left(-\lambda^I_{r_2}\alpha\Phi(k')+\lambda^K_{r_2}\beta\Psi(k')\right)=\lambda^S_\sigma\Psi(k'_\sigma)+\lambda^S_\mu\Psi(k'_\mu), \tag{D 1i}$$
$$\varphi_\sigma^{-1}\varphi_\mu^{-1}\left(\lambda^I_{\theta_1}\Phi(k)-\lambda^K_{\theta_1}\Psi(k)\right)=\lambda^R_\sigma\Phi(k_\sigma), \tag{D 1j}$$
$$\begin{aligned}\varphi_\sigma^{-1}\varphi_\mu^{-1}\left(\lambda^I_{\theta_1}\alpha_1\Phi(k_1)-\lambda^K_{\theta_1}\beta_1\Psi(k_1)\right)-\tilde{\Omega}\left(\lambda^I_{r_1}\alpha_1+\lambda^K_{r_1}\beta_1\right)\\ =\varphi_\sigma^{-1}\varphi_\mu^{-1}\left(\lambda^I_{\theta_2}\Phi(k_1)-\lambda^K_{\theta_2}\Psi(k_1)\right),\end{aligned} \tag{D 1k}$$
$$\varphi_\sigma^{-1}\varphi_\mu^{-1}\left(\lambda^I_{\theta_2}\alpha\Phi(k')-\lambda^K_{\theta_2}\beta\Psi(k')\right)=-\lambda^S_\sigma\Psi(k'_\sigma). \tag{D 1l}$$

with

$$k_1=(1+e_1)k,\quad (k',k'_\sigma,k'_\mu)=(1+e)(k,k_\sigma,k_\mu), \tag{D 2a}$$
$$k_\sigma=k\left(\tfrac{1+\sigma}{1+\sigma s^2}\right)^{1/2},\quad k_\mu=k\left(\tfrac{1+\mu}{1+\mu s^2}\right)^{1/2}, \tag{D 2b}$$
$$\tilde{\Omega}=\Omega\tfrac{s}{c}(1+e_1)^2,\quad \Phi(x)=x\tfrac{I_0(x)}{I_1(x)},\quad \Psi(x)=x\tfrac{K_0(x)}{K_1(x)}, \tag{D 2c}$$
$$\alpha_1=\tfrac{I_1(k_1)}{I_1(k)},\quad \beta_1=\tfrac{K_1(k_1)}{K_1(k)},\quad \alpha'=\tfrac{I_1(k')}{I_1(k)},\quad \beta'=\tfrac{K_1(k')}{K_1(k)},\quad \alpha=\tfrac{\alpha'}{\alpha_1},\quad \beta=\tfrac{\beta'}{\beta_1}. \tag{D 2d}$$

The system (D 1$a-l$) is thus represented by the following 12 $\times$ 12 matrix

$$\begin{bmatrix}
1 & 1 & -1 & -1 & 0 & 0 & 0 & 0 & 0 & 0 & 0 & 0 \\
-1 & 0 & 0 & 0 & \varphi_\mu^{-1} & \varphi_\mu^{-1} & 0 & 0 & 0 & 0 & 0 & 0 \\
\Phi(k_\sigma) & \Phi(k_\mu) & -\varphi_\mu^{-1}\Phi(k) & \varphi_\mu^{-1}\Psi(k) & 0 & 0 & 0 & 0 & 0 & 0 & 0 & 0 \\
0 & 0 & \alpha_1 & \beta_1 & 0 & 0 & -1 & -1 & 0 & 0 & 0 & 0 \\
0 & 0 & 0 & 0 & \alpha_1 & \beta_1 & 0 & 0 & -1 & -1 & 0 & 0 \\
0 & 0 & \alpha_1\Phi(k_1) & -\beta_1\Psi(k_1) & 0 & 0 & -\Phi(k_1) & \Psi(k_1) & 0 & 0 & 0 & 0 \\
0 & 0 & 0 & 0 & 0 & 0 & \alpha & \beta & 0 & 0 & -1 & -1 \\
0 & 0 & 0 & 0 & 0 & 0 & 0 & 0 & \varphi_\mu^{-1}\alpha & \varphi_\mu^{-1}\beta & -1 & 0 \\
0 & 0 & 0 & 0 & 0 & 0 & \varphi_\mu^{-1}\alpha\Phi(k') & -\varphi_\mu^{-1}\beta\Psi(k') & 0 & 0 & \Psi(k'_\sigma) & \Psi(k'_\mu) \\
-\Phi(k_\sigma) & 0 & 0 & 0 & a\Phi(k) & -a\Psi(k) & 0 & 0 & 0 & 0 & 0 & 0 \\
0 & 0 & \alpha_1\tilde{\Omega} & \beta_1\tilde{\Omega} & -a\alpha_1\Phi(k_1) & a\beta_1\Psi(k_1) & 0 & 0 & a\Phi(k_1) & -a\Psi(k_1) & 0 & 0 \\
0 & 0 & 0 & 0 & 0 & 0 & 0 & 0 & a\alpha\Phi(k') & -a\beta\Psi(k') & \Psi(k'_\sigma) & 0
\end{bmatrix}. \tag{D 3}$$

with $a = \varphi_\sigma^{-1}\varphi_\mu^{-1}$. As (D 1$a-l$) must be singular, the determinant of this matrix must be set to zero. Then, by making linear combinations of lines or columns (where c_n and l_m mean column n and line m respectively), we will simplify this determinant in a succession of steps, at each step the determinant being equal to zero. First let us swap c_1 and c_2, add $\alpha_1 c_7$ to c_3, add $\beta_1 c_8$ to c_4, add $\alpha_1 c_9$ to c_5 and then multiply the new column c_5 by φ_μ, add $\beta_1 c_{10}$ to c_6 and then multiply the new column c_6 by φ_μ, subtract c_7 to c_8, multiply c_9 by α_1 and c_{10} by β_1, and finally subtract the new line l_1 multiplied by $\Phi(k_\mu)$ to the new line l_3. This leads to the following 9 $\times$ 9 determinant

$$\begin{vmatrix}
-1 & 0 & 0 & 1 & 1 & 0 & 0 & 0 & 0 \\
E_{\sigma\mu} & A(\mu) & B(\mu) & 0 & 0 & 0 & 0 & 0 & 0 \\
0 & 0 & 0 & 0 & 0 & -\alpha_1 & -\beta_1 & 0 & 0 \\
0 & \alpha' & \beta' & 0 & 0 & 0 & 0 & -1 & -1 \\
0 & 0 & 0 & \alpha' & \beta' & \varphi_\mu^{-1}\alpha' & \varphi_\mu^{-1}\beta' & -1 & 0 \\
0 & \varphi_\mu^{-1}\alpha'\Phi(k') & -\varphi_\mu^{-1}\beta'\Psi(k') & 0 & 0 & 0 & 0 & \Psi(k'_\sigma) & \Psi(k'_\mu) \\
-\Phi(k_\sigma) & 0 & 0 & \varphi_\sigma^{-1}\Phi(k) & -\varphi_\sigma^{-1}\Psi(k) & 0 & 0 & 0 & 0 \\
0 & \alpha_1\tilde{\Omega} & \beta_1\tilde{\Omega} & 0 & 0 & a\alpha_1\Phi(k_1) & -a\beta_1\Psi(k_1) & 0 & 0 \\
0 & 0 & 0 & \varphi_\sigma^{-1}\alpha'\Phi(k') & -\varphi_\sigma^{-1}\beta'\Psi(k') & a\alpha'\Phi(k') & -a\beta'\Psi(k') & \Psi(k'_\sigma) & 0
\end{vmatrix} = 0, \quad \text{(D 4)}$$

where $E_{\sigma\mu} = \Phi(k_\sigma) - \Phi(k_\mu)$, $A(\nu) = \Phi(k_\nu) - \varphi_\nu^{-1}\Phi(k)$ and $B(\nu) = \Phi(k_\nu) + \varphi_\nu^{-1}\Psi(k)$. Then, multiplying columns c_6 and c_7 by φ_μ and dividing line l_3 by φ_μ, thus adding c_1 to c_4, adding c_1 to c_5, adding $\Psi(k'_\mu)l_4$ to l_6, leads to the 7×7 determinant

$$\begin{vmatrix} A(\mu) & B(\mu) & E_{\sigma\mu} & E_{\sigma\mu} & 0 & 0 & 0 \\ 0 & 0 & 0 & 0 & -\alpha_1 & -\beta_1 & 0 \\ 0 & 0 & \alpha' & \beta' & \alpha' & \beta' & -1 \\ \alpha' C(\mu) & \beta' D(\mu) & 0 & 0 & 0 & 0 & F_{\sigma\mu} \\ 0 & 0 & -A(\sigma) & -B(\sigma) & 0 & 0 & 0 \\ \alpha_1\tilde{\Omega} & \beta_1\tilde{\Omega} & 0 & 0 & \varphi_\sigma^{-1}\alpha_1\Phi(k_1) & -\varphi_\sigma^{-1}\beta_1\Psi(k_1) & 0 \\ 0 & 0 & \varphi_\sigma^{-1}\alpha'\Phi(k') & -\varphi_\sigma^{-1}\beta'\Psi(k') & \varphi_\sigma^{-1}\alpha'\Phi(k') & -\varphi_\sigma^{-1}\beta'\Psi(k') & \Psi(k'_\sigma) \end{vmatrix} = 0, \tag{D 5}$$

where $C(\nu) = \Psi(k'_\nu) + \varphi_\nu^{-1}\Phi(k')$, $D(\nu) = \Psi(k'_\nu) - \varphi_\nu^{-1}\Psi(k')$ and $F_{\sigma\mu} = \Psi(k'_\sigma) - \Psi(k'_\mu)$. Then subtracting c_5 to c_3, subtracting c_6 to c_4, adding $\alpha' c_7$ to c_5, adding $\beta' c_7$ to c_6, leads to the 6×6 determinant

$$\begin{vmatrix} A(\mu) & B(\mu) & E_{\sigma\mu} & E_{\sigma\mu} & 0 & 0 \\ 0 & 0 & \alpha_1 & \beta_1 & -\alpha_1 & -\beta_1 \\ \alpha' C(\mu) & \beta' D(\mu) & 0 & 0 & \alpha' F_{\sigma\mu} & \beta' F_{\sigma\mu} \\ 0 & 0 & -A(\sigma) & -B(\sigma) & 0 & 0 \\ \alpha_1\tilde{\Omega} & \beta_1\tilde{\Omega} & -\varphi_\sigma^{-1}\alpha_1\Phi(k_1) & \varphi_\sigma^{-1}\beta_1\Psi(k_1) & \varphi_\sigma^{-1}\alpha_1\Phi(k_1) & -\varphi_\sigma^{-1}\beta_1\Psi(k_1) \\ 0 & 0 & 0 & 0 & \alpha' C(\sigma) & \beta' D(\sigma) \end{vmatrix} = 0. \tag{D 6}$$

Then, multiplying c_3, c_4, c_5 and c_6 by φ_μ^{-1}, multiplying l_1, l_2 and l_3 by φ_μ, multiplying l_4, l_5 and l_6 by $\varphi_\sigma\varphi_\mu$, dividing c_1, c_3 and c_5 by α_1, dividing c_2, c_4 and c_6 by β_1, dividing l_1 and l_4 by $E_{\sigma\mu}$, dividing l_3 and l_6 by $F_{\sigma\mu}$, leads to

$$\begin{vmatrix} \bar{A}(\mu) & \bar{B}(\mu) & \alpha_1^{-1} & \beta_1^{-1} & 0 & 0 \\ 0 & 0 & 1 & 1 & -1 & -1 \\ \bar{C}(\mu) & \bar{D}(\mu) & 0 & 0 & \alpha & \beta \\ 0 & 0 & -\bar{A}(\sigma) & -\bar{B}(\sigma) & 0 & 0 \\ \Omega^{**} & \Omega^{**} & -\Phi(k_1) & \Psi(k_1) & \Phi(k_1) & -\Psi(k_1) \\ 0 & 0 & 0 & 0 & \bar{C}(\sigma) & \bar{D}(\sigma) \end{vmatrix} = 0, \tag{D 7}$$

where $\bar{A}(\nu) = E_{\sigma\mu}^{-1}\alpha_1^{-1}\varphi_\nu A(\nu)$, $\bar{B}(\nu) = E_{\sigma\mu}^{-1}\beta_1^{-1}\varphi_\nu B(\nu)$, $\bar{C}(\nu) = F_{\sigma\mu}^{-1}\alpha\varphi_\nu C(\nu)$, $\bar{D}(\nu) = F_{\sigma\mu}^{-1}\beta\varphi_\nu D(\nu)$ and $\Omega^{**} = \varphi_\sigma\varphi_\mu\tilde{\Omega}$. Then, adding c_5 to c_3, adding c_6 to c_4, subtracting c_6 to c_5, leads to the 5×5 determinant

$$\begin{vmatrix} \bar{A}(\mu) & \bar{B}(\mu) & \alpha_1^{-1} & \beta_1^{-1} & 0 \\ \bar{C}(\mu) & \bar{D}(\mu) & \alpha & \beta & \alpha - \beta \\ 0 & 0 & -\bar{A}(\sigma) & -\bar{B}(\sigma) & 0 \\ \bar{\Omega} & \bar{\Omega} & 0 & 0 & 1 \\ 0 & 0 & \bar{C}(\sigma) & \bar{D}(\sigma) & \bar{C}(\sigma) - \bar{D}(\sigma) \end{vmatrix} = 0, \tag{D 8}$$

where $\bar{\Omega} = \Omega^{**}(\Phi(k_1) + \Psi(k_1))^{-1}$. Then, subtracting c_2 to c_1, and then subtracting $\frac{\bar{A}(\mu)-\bar{B}(\mu)}{\bar{C}(\mu)-\bar{D}(\mu)} l_2$ to l_1, leads to the 4×4 determinant

$$\begin{vmatrix} \bar{B}(\mu) - \frac{\bar{A}(\mu)-\bar{B}(\mu)}{\bar{C}(\mu)-\bar{D}(\mu)}\bar{D}(\mu) & \frac{1}{\alpha_1} - \frac{\bar{A}(\mu)-\bar{B}(\mu)}{\bar{C}(\mu)-\bar{D}(\mu)}\alpha & \frac{1}{\beta_1} - \frac{\bar{A}(\mu)-\bar{B}(\mu)}{\bar{C}(\mu)-\bar{D}(\mu)}\beta & -(\alpha-\beta)\frac{\bar{A}(\mu)-\bar{B}(\mu)}{\bar{C}(\mu)-\bar{D}(\mu)} \\ 0 & -\bar{A}(\sigma) & -\bar{B}(\sigma) & 0 \\ \bar{\Omega} & 0 & 0 & 1 \\ 0 & \bar{C}(\sigma) & \bar{D}(\sigma) & \bar{C}(\sigma) - \bar{D}(\sigma) \end{vmatrix} = 0. \tag{D 9}$$

Then, multiplying l_1 by $\bar{C}(\mu) - \bar{D}(\mu)$ and subtracting ($\bar{B}(\sigma)c_2$ to c_3 times $\bar{A}(\sigma)$), leads to the 3 × 3 determinant

$$\begin{vmatrix} \begin{array}{c}\bar{B}(\mu)\bar{C}(\mu)- \\ \bar{A}(\mu)\bar{D}(\mu)\end{array} & \begin{array}{c}(\bar{C}(\mu)-\bar{D}(\mu))(\frac{\bar{A}(\sigma)}{\beta_1}-\frac{\bar{B}(\sigma)}{\alpha_1})+ \\ (\bar{A}(\mu)-\bar{B}(\mu))(-\beta\bar{A}(\sigma)+\alpha\bar{B}(\sigma))\end{array} & -(\alpha-\beta)(\bar{A}(\mu)-\bar{B}(\mu)) \\ \bar{\Omega} & 0 & 1 \\ 0 & \bar{D}(\sigma)\bar{A}(\sigma)-\bar{B}(\sigma)\bar{C}(\sigma) & \bar{C}(\sigma)-\bar{D}(\sigma) \end{vmatrix} = 0. \tag{D 10}$$

After developing this determinant, the following expression of Ω can be derived

$$\Omega = -\frac{c}{s}\frac{1}{(1+e_1)^2}\frac{(\Phi(k_1)+\Psi(k_1))P(\sigma)P(\mu)}{E_{\sigma\mu}Q(\sigma)Q(\mu)\frac{\Phi(k)+\Psi(k)}{\alpha_1\beta_1}+F_{\sigma\mu}R(\sigma)R(\mu)\alpha\beta(\Phi(k')+\Psi(k'))}, \tag{D 11}$$

with the notations given in $(5.4a-f)$. Then, using $(\mathrm{A}\,2a,b)$ leads to (5.3).

Appendix E. Relations between cases (b) and (c) for $e_1 \gg 1$

Denoting the parameters relating to cases (b) and (c) with an exponent b or c, we have the following dimensional relations

$$R^c + \bar{e}_1 = R^b, \quad R^c + \bar{e}^c = R^b + \bar{e}^b, \tag{E 1}$$

where $\bar{e}_1 = R^c e_1$, $\bar{e}^c = R^c e^c$ and $\bar{e}^b = R^b e^b$. It implies

$$R^c(1+e_1) = R^b, \quad R^c(1+e^c) = R^b(1+e^b), \tag{E 2}$$

and therefore

$$1+e^b = \frac{1+e^c}{1+e_1}. \tag{E 3}$$

In addition, assuming the same magnetic vertical wavelength H in both cases (b) and (c), we have

$$k^b\frac{H}{R^b} = k^c\frac{H}{R^c}, \tag{E 4}$$

implying from (E 2) that

$$k^b = k^c(1+e_1). \tag{E 5}$$

From their definition,

$$k'^b = (1+e^b)k^b, \quad k'^c = (1+e^c)k^c, \tag{E 6}$$

implying that

$$\frac{k'^b}{k'^c} = \left(\frac{1+e^b}{1+e^c}\right)\frac{k^b}{k^c}. \tag{E 7}$$

Then, using (E 3) and (E 5), (E 7) leads to $k'^b = k'^c$.

Appendix F. Correspondence between Ω_{2025} given by (6.10) and $\Omega^{(c)}$

We demonstrate equation (6.10) which is obtained from equation (47) of Plunian *et al.* (2025). In Plunian *et al.* (2025), the dispersion relation takes the form

$$\overline{\Omega^c} = \frac{F_\mu F_\sigma - \overline{\omega}\left[-M_{\mu\sigma}E_\mu E_\sigma + L_{\mu\sigma}(DBA'-BCB')\right]}{M_{\mu\sigma}(DBA'-BCB') - L_{\mu\sigma}(B'+K_\mu D)(B'+K_\sigma D) - M_{\mu\sigma}L_{\mu\sigma}D^2\overline{\omega}}, \tag{F 1}$$

with

$$\overline{\Omega^c} = \varphi_\mu\varphi_\sigma(\Omega^{(c)} - \omega)\tfrac{s}{c},\ \overline{\omega} = \varphi_\mu\varphi_\sigma\omega\tfrac{s}{c}(1+e),\ A = k\tfrac{I_0(k)}{I_1(k)},\ B = k\left(\tfrac{I_0(k)}{I_1(k)} + \tfrac{K_0(k)}{K_1(k)}\right), \tag{F 2a}$$

$$C = \tfrac{I_1(k')}{I_1(k)},\quad D = \tfrac{I_1(k')}{I_1(k)} - \tfrac{K_1(k')}{K_1(k)},\quad A' = k\tfrac{I_0(k')}{I_1(k)},\quad B' = k\left(\tfrac{I_0(k')}{I_1(k)} + \tfrac{K_0(k')}{K_1(k)}\right), \tag{F 2b}$$

$$I_\nu = k_\nu\varphi_\nu\tfrac{I_0(k_\nu)}{I_1(k_\nu)},\quad K_\nu = k_\nu\varphi_\nu\tfrac{K_0(k'_\nu)}{K_1(k'_\nu)}, \tag{F 2c}$$

$$L_{\mu\sigma} = \varphi_\sigma^{-1}I_\sigma - \varphi_\mu^{-1}I_\mu,\quad M_{\mu\sigma} = \varphi_\sigma^{-1}K_\sigma - \varphi_\mu^{-1}K_\mu, \tag{F 2d}$$

$$E_\nu = AD - BC - DI_\nu,\quad F_\nu = B(A' + K_\nu C) - (B' + K_\nu D)(A - I_\nu), \tag{F 2e}$$

$$k' = (1+e)k,\quad k'_\nu = (1+e)k_\nu. \tag{F 2f}$$

The correspondence with the notations given in $(5.4a-f)$ and $(6.9a,b)$ are the following

$$\Omega^{(c)} = \Omega_{2025},\quad A = \Phi(k),\quad B = \Phi(k) + \Psi(k),\quad C = \alpha',\quad D = \alpha' - \beta', \tag{F 3a}$$

$$A' = \frac{\alpha'}{1+e}\Phi(k'), B' = \frac{1}{1+e}\left(\alpha'\Phi(k') + \beta'\Psi(k')\right), I_\nu = \varphi_\nu\Phi(k_\nu), K_\nu = \frac{\varphi_\nu}{1+e}\Psi(k'_\nu), \tag{F 3b}$$

$$L_{\mu\sigma} = E_{\sigma\mu},\quad M_{\mu\sigma} = \frac{F_{\sigma\mu}}{1+e},\quad E_\nu = \varphi_\nu M(\nu),\quad F_\nu = -\frac{\varphi_\nu^2}{1+e}L(\nu). \tag{F 3c}$$

To obtain (6.10) we also use the relations (A 7) and (A 8).

Appendix G. Derivation of J_r and J_θ

The horizontal components of the electric current density are derived from $(2.9c)$, leading to the following expressions

$$J_r = -ik\tilde{\varphi}_\mu^{-1}\tilde{\phi}, \tag{G 1a}$$

$$J_\theta = ik^{-1}\tilde{\varphi}_\mu^{-1}[D_k(B_r) + \tilde{\mu}c^2k^2B_r + \tilde{\mu}csk^2B_\theta], \tag{G 1b}$$

with $\tilde{\phi}$ defined in (4.18b). At the dynamo threshold $\gamma = 0$, equation $(2.14a)$ implies that

$$D_k(B_r) = (1+\tilde{\sigma}s^2)^{-1}\left[cs(\tilde{\sigma} - \tilde{\mu})k^2B_\theta - \tilde{\mu}c^2k^2B_r\right], \tag{G 2}$$

then leading to

$$J_\theta = ik\frac{cs\tilde{\sigma}}{1+s^2\tilde{\sigma}}\tilde{\varphi}_\mu^{-1}\tilde{\phi}. \tag{G 3}$$

For each case (a), (b) and (c), the expressions of J_r and J_θ given in $(\mathrm{G}\,1a)$ and (G 3) are then derived from $\tilde{\phi}$ given in (4.19-4.21). We note that $(\mathrm{G}\,1a)$ and (G 3) lead to the following relation

$$(1+s^2\tilde{\sigma})J_\theta + cs\tilde{\sigma}J_r = 0, \tag{G 4}$$

corresponding to logarithmic spiral lines for $\tilde{\sigma} \neq 0$ and radial lines for $\tilde{\sigma} = 0$.

Appendix H. Derivation of B_z

The expression of $B_z(r)$ can be derived from (3.6), that can be rewritten as

$$B_z = ik^{-1}\frac{1}{r}\partial_r(rB_r). \tag{H 1}$$

Applying the relations $\partial_r(rI_1(\nu r)) = \nu r I_0(\nu r)$ and $\partial_r(rK_1(\nu r)) = -\nu r K_0(\nu r)$ to (4.9) for case (a), (4.11) for case (b), and (4.13) for case (c), leads to

$$B_z^{(a)} = ik^{-1}\begin{cases} r<1, & -s\left(\lambda_\sigma^R k_\sigma \dfrac{I_0(k_\sigma r)}{I_1(k_\sigma)} + \lambda_\mu^R k_\mu \dfrac{I_0(k_\mu r)}{I_1(k_\mu)}\right) \\ 1<r<1+e & -sk\left(\lambda_r^I \dfrac{I_0(kr)}{I_1(k)} - \lambda_r^K \dfrac{K_0(kr)}{K_1(k)}\right) \\ r>1+e, & s\lambda_r^S k \dfrac{K_0(kr)}{K_1(k(1+e))} \end{cases}, \tag{H 2}$$

$$B_z^{(b)} = ik^{-1}\begin{cases} r<1, & -s\lambda_r^R k \dfrac{I_0(kr)}{I_1(k)} \\ 1<r<1+e & -sk\left(\lambda_r^I \dfrac{I_0(kr)}{I_1(k)} - \lambda_r^K \dfrac{K_0(kr)}{K_1(k)}\right) \\ r>1+e, & s\left(\lambda_\sigma^S k_\sigma \dfrac{K_0(k_\sigma r)}{K_1(k_\sigma(1+e))} + \lambda_\mu^S k_\mu \dfrac{K_0(k_\mu r)}{K_1(k_\mu(1+e))}\right) \end{cases}, \tag{H 3}$$

$$B_z^{(c)} = ik^{-1}\begin{cases} r<1, & -s\left(\lambda_\sigma^R k_\sigma \dfrac{I_0(k_\sigma r)}{I_1(k_\sigma)} + \lambda_\mu^R k_\mu \dfrac{I_0(k_\mu r)}{I_1(k_\mu)}\right) \\ 1<r<1+e_1 & -sk\left(\lambda_{r1}^I \dfrac{I_0(kr)}{I_1(k)} - \lambda_{r1}^K \dfrac{K_0(kr)}{K_1(k)}\right) \\ 1+e_1<r<1+e & -sk\left(\lambda_{r2}^I \dfrac{I_0(kr)}{I_1(k(1+e_1))} - \lambda_{r2}^K \dfrac{K_0(kr)}{K_1(k(1+e_1))}\right) \\ r>1+e, & s\left(\lambda_\sigma^S k_\sigma \dfrac{K_0(k_\sigma r)}{K_1(k_\sigma(1+e))} + \lambda_\mu^S k_\mu \dfrac{K_0(k_\mu r)}{K_1(k_\mu(1+e))}\right) \end{cases}. \tag{H 4}$$